ISSN 2523-6776

Volume 5, Issue 15 – January – June - 2021

Journal of Technological Engineering

ECORFAN®

Journal of Technological Engineering, Volume 5, Issue 15, January - June 2021, is a journal edited six monthly by ECORFAN-Taiwan. Taiwan, Taipei. YongHe district, ZhongXin, Street 69. Postcode: 23445. WEB: www.ecorfan.org/taiwan, revista@ecorfan.org. Chief Editor: SERRUDO-GONZALES, Javier. BsC. ISSN-On line: 2523-6776. Responsible for the latest update of this number ECORFAN Computer Unit. ESCAMILLA-BOUCHÁN, Imelda, PhD, LUNA-SOTO, Vladimir. PhD. Taiwan, Taipei. YongHe district, ZhongXin, Street 69, last updated June 30, 2021.

Journal of Technological Engineering

Definition of Journal

Scientific Objectives

Support the international scientific community in its written production Science, Technology and Innovation in the Field of Engineering and Technology, in Subdisciplines of electromagnetism, electrical distribution, sources innovation in electrical, engineering signal, amplification electrical, motor design science, materials in electrical power, plants management and distribution of electrical energies.

ECORFAN-Mexico SC is a Scientific and Technological Company in contribution to the Human Resource training focused on the continuity in the critical analysis of International Research and is attached to CONACYT-RENIECYT number 1702902, its commitment is to disseminate research and contributions of the International Scientific Community, academic institutions, agencies and entities of the public and private sectors and contribute to the linking of researchers who carry out scientific activities, technological developments and training of specialized human resources with governments, companies and social organizations.

Encourage the interlocution of the International Scientific Community with other Study Centers in Mexico and abroad and promote a wide incorporation of academics, specialists and researchers to the publication in Science Structures of Autonomous Universities - State Public Universities - Federal IES - Polytechnic Universities - Technological Universities - Federal Technological Institutes - Normal Schools - Decentralized Technological Institutes - Intercultural Universities - S & T Councils - CONACYT Research Centers.

Scope, Coverage and Audience

Journal of Technological Engineering is a Journal edited by ECORFAN-Mexico S.C in its Holding with repository in Taiwan, is a scientific publication arbitrated and indexed with semester periods. It supports a wide range of contents that are evaluated by academic peers by the Double-Blind method, around subjects related to the theory and practice of electromagnetism, electrical distribution, sources innovation in electrical, engineering signal, amplification electrical, motor design science, materials in electrical power, plants management and distribution of electrical energies with diverse approaches and perspectives, that contribute to the diffusion of the development of Science Technology and Innovation that allow the arguments related to the decision making and influence in the formulation of international policies in the Field of Engineering and Technology. The editorial horizon of ECORFAN-Mexico® extends beyond the academy and integrates other segments of research and analysis outside the scope, as long as they meet the requirements of rigorous argumentative and scientific, as well as addressing issues of general and current interest of the International Scientific Society.

Editorial Board

Arbitration Committee

Assignment of Rights

The sending of an Article to Journal of Systematic Innovation emanates the commitment of the author not to submit it simultaneously to the consideration of other series publications for it must complement the Originality Format for its Article.

The authors sign the Authorization Format for their Article to be disseminated by means that ECORFAN-Mexico, S.C. In its Holding Taiwan considers pertinent for disclosure and diffusion of its Article its Rights of Work.

Declaration of Authorship

Indicate the Name of Author and Coauthors at most in the participation of the Article and indicate in extensive the Institutional Affiliation indicating the Department.

Identify the Name of Author and Coauthors at most with the CVU Scholarship Number-PNPC or SNI-CONACYT- Indicating the Researcher Level and their Google Scholar Profile to verify their Citation Level and H index.

Identify the Name of Author and Coauthors at most in the Science and Technology Profiles widely accepted by the International Scientific Community ORC ID - Researcher ID Thomson - arXiv Author ID - PubMed Author ID - Open ID respectively.

Indicate the contact for correspondence to the Author (Mail and Telephone) and indicate the Researcher who contributes as the first Author of the Article.

Plagiarism Detection

All Articles will be tested by plagiarism software PLAGSCAN if a plagiarism level is detected Positive will not be sent to arbitration and will be rescinded of the reception of the Article notifying the Authors responsible, claiming that academic plagiarism is criminalized in the Penal Code.

Arbitration Process

All Articles will be evaluated by academic peers by the Double Blind method, the Arbitration Approval is a requirement for the Editorial Board to make a final decision that will be final in all cases. MARVID® is a derivative brand of ECORFAN® specialized in providing the expert evaluators all of them with Doctorate degree and distinction of International Researchers in the respective Councils of Science and Technology the counterpart of CONACYT for the chapters of America-Europe-Asia- Africa and Oceania. The identification of the authorship should only appear on a first removable page, in order to ensure that the Arbitration process is anonymous and covers the following stages: Identification of the Journal with its author occupation rate - Identification of Authors and Coauthors - Detection of plagiarism PLAGSCAN - Review of Formats of Authorization and Originality-Allocation to the Editorial Board-Allocation of the pair of Expert Arbitrators-Notification of Arbitration -Declaration of observations to the Author-Verification of Article Modified for Editing-Publication.

Instructions for Scientific, Technological and Innovation Publication

Knowledge Area

The works must be unpublished and refer to topics of Electromagnetism, Electrical distribution, Sources innovation in electrical, Engineering signal, Amplification electrical, Motor design science, Materials in electrical power, Plants management and distribution of electrical energies and other topics related to Engineering and Technology.

Presentation of the content

In the first article we present, *Graphical user interface for the patterns detection in wine crops*, by JARA-RUIZ, Ricardo, RODRÍGUEZ-PADILLA, Luis Ángel, LÓPEZ-ÁLVAREZ, Yadira Fabiola, and RODRÍGUEZ-FRANCO, Martín Eduardo, with adscription in the Universidad Tecnológica del Norte de Aguascalientes, in the next article we present, *Drag and lift force analysis for the cybertruck Tesla vehicle*, by HORTELANO-CAPETILLO, Juan Gregorio, MARTÍNEZ-VÁZQUEZ, J. Merced, BAÑOS-LOPEZ, Esperanza and ALFARO-AYALA J. Arturo, with adscription in the Universidad Politécnica de Juventino Rosas, Universidad Autónoma del Estado de Hidalgo and the Universidad de Guanajuato, in the next article we present, *Direct design process of aerodynamic profiles using the Joukowsky transformation*, by ROMERO-GÓMEZ, Gabriel Adrián & LÓPEZ-GARZA, Víctor, with adscription in the Universidad Michoacana de San Nicolás de Hidalgo, in the last article we present, *Mathematical modeling of a MOSFET transistor as modulator in AM transmission*, by MOTA-GALVÁN, Eduardo & REYES-MARTINEZ, Roberto Alejandro, with adscription in the Universidad Autónoma de Baja California.

Content

Article **Journal of Technological Engineering**
June, 2021 Vol.5 No.15 1-8

Graphical user interface for the patterns detection in wine crops

Interfaz gráfica de usuario para la detección de patrones en cultivos vinícolas

JARA-RUIZ, Ricardo†*, RODRÍGUEZ-PADILLA, Luis Ángel, LÓPEZ-ÁLVAREZ, Yadira Fabiola, and RODRÍGUEZ-FRANCO, Martín Eduardo

Universidad Tecnológica del Norte de Aguascalientes, Av. Universidad No. 1001, Estación Rincón, Rincón de Romos, Ags. C.P. 20400.

ID 1st Author: *Ricardo, Jara-Ruiz* / **ORC ID**: 0000-0001-7725-4138, **Researcher ID Thomson**: T-1532-2018, **CVU CONACYT ID**: 630276

ID 1st Coauthor: *Luis Ángel, Rodríguez-Padilla* / **ORC ID**: 0000-0003-1578-8569, **CVU CONACYT ID**: 1046926

ID 2nd Coauthor: *Yadira Fabiola, López-Álvarez* / **ORC ID**: 0000-0002-9041-1908, **Researcher ID Thomson**: T-1555-2018, **CVU CONACYT ID**: 375952

ID 3rd Coauthor: *Martín Eduardo, Rodríguez-Franco* / **ORC ID**: 0000-0002-6804-4777, **Researcher ID Thomson**: T-1539-2018, **CVU CONACYT ID**: 660892

DOI: 10.35429/JTEN.2021.15.5.1.8 Received March 14, 2021; Accepted June 29, 2021

Abstract

Considering that our country has an important participation in the grape productive sector for this reason it is one of the crops with the best opportunity areas for the implementation of this technology type. In this paper the design and development of a Graphical User Interface (GUI) generated in the MATLAB programming environment is exposed, through which the pictures acquisition and process from interest information is carried out to implement patter recognition strategies in the wine crops agroindustrial sector to monitor and generate a timely diagnostic of its currently status. The GUI has a section than allows the pictures acquisition in real time to later capture the information to be processed and through the application of filters and color recognition techniques on the crop leaf (study object) it's processed to establish a diagnostic, which will allow the user to apply the appropriate measures contributing in the best way to a crop optimal development.

Graphical User Interface, Pattern detection and Wine crops

Resumen

Nuestro país se caracteriza por tener una importante participación en el sector productivo de la uva y considerado uno de los cultivos con mejores áreas de oportunidad para la implementación de este tipo de tecnología. En el presente trabajo de investigación se expone el diseño y desarrollo de una interfaz gráfica de usuario (GUI) generada en el entorno de programación MATLAB, a través de la cual se realiza la adquisición y procesamiento de imágenes considerando datos de interés con el propósito de implementar estrategias de reconocimiento de patrones con un enfoque hacía el sector agroindustrial, específicamente en los cultivos vinícolas permitiendo monitorear y generar un diagnóstico oportuno del estado actual del mismo. La GUI cuenta con una sección que permite la adquisición de imágenes en tiempo real para posteriormente capturar la información a procesar y por medio de la aplicación de filtros y técnicas de reconocimiento de colores en la hoja del cultivo (objeto de estudio) se procesa para establecer un diagnóstico, lo que permitirá al usuario aplicar las medidas permitentes contribuyendo de la mejor manera a un óptimo desarrollo del cultivo.

Interfaz Gráfica de Usuario, Detección de patrones y Cultivos vinícolas

Citation: JARA-RUIZ, Ricardo, RODRÍGUEZ-PADILLA, Luis Ángel, LÓPEZ-ÁLVAREZ, Yadira Fabiola, and RODRÍGUEZ-FRANCO, Martín Eduardo. Graphical user interface for the patterns detection in wine crops. Journal of Technological Engineering. 2021. 5-15: 1-8

* Correspondence to Author (e-mail: ricardo.jara@utna.edu.mx)
† Researcher contributing as first author.

Introduction

The field of image processing is continually evolving. In recent years there has been a significant increase in interest in fields such as image morphology, artificial neural networks, color and / or grayscale image processing, image data understanding, image recognition, and knowledge-based analysis systems. .

At present, automation in the wine sector tends to replace the hand of man in some of its operational processes, in order to increase productivity and reduce the risk of physical exposure represented by human participation, but there is still a great gap in activities that require emulating the five senses of man, which have as a common purpose the recognition of patterns.

As a solution to the indicated problem, the development of a graphical user interface in the MATLAB programming environment is presented that allows the acquisition of images and their processing by means of pattern recognition and color detection techniques to generate a timely diagnosis. of the current state of the crop to study.

Graphical User Interface

The graphic interface is the "space" or "surface" that connects or articulates the interaction between the human being (user) with the artifact (computer) and the objective of an action (teaching-learning). The objective of the graphical interface is to make the communicative content of the information accessible. (Rivera, 2005)

MATLAB software

The MATLAB platform is optimized for solving scientific and engineering problems. The matrix-based language of MATLAB is the world's most natural way to express computational mathematics. Integrated graphs make it easy to view data and obtain information from it. A vast library of built-in Toolboxes lets you immediately get started with essential algorithms for your domain. The desktop environment invites you to experiment, explore and discover. All of these MATLAB tools and functions are rigorously tested and designed to work together.. (MathWorks, 2020)

Image processing.

The digital processing or treatment of images consists of algorithmic processes that transform one image into another where certain information of interest is highlighted, and / or irrelevant information for the application is attenuated or eliminated. Thus, the tasks of image processing include the suppression of noise, contrast enhancements, elimination of unwanted effects in the capture such as blurring or distortions due to optical or movement effects, geometric mappings, color transformations, etc. (Moya, 2012)

Geometric transformations.

They are carried out taking into account the positions of the pixels in the image, and translation / rotation operations are applied to them (Figure 1). Typical examples are rotation, translation, scaling, and pixel rectification. (Dobernack)

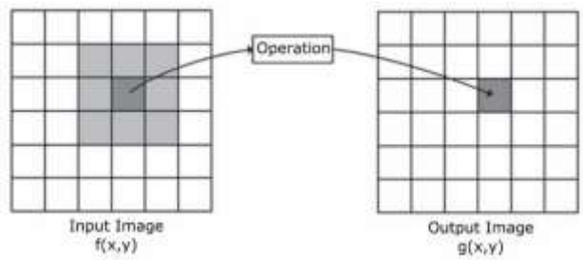

Figure 1 Spatial transformation.
Source: (Dobernack)

Color segmentation

The multispectral segmentation tool uses the RGB image format and its operation is similar to segmentation by thresholds. The only notable difference is that three groups of thresholds must be established, one for each of the spectral bands, which are applied to the corresponding red, green and blue layers that make up the color image. (Grau, 2010)

Artificial vision

Artificial Vision or also called Computer Vision, aims to capture visual information from the physical environment to extract relevant visual characteristics, using automatic procedures. According to Marr, "Vision is a process that produces a useful description for the observer from images of the outside world and does not have irrelevant information". (Dueñas, 2009)

ISSN 2523-6776

Methodology

Problem Statement

There is a great gap in the development of applications that require emulating the five senses of man in the vine sector, which have as a common purpose the recognition of patterns from the leaf. Therefore, the lack of taking advantage of the advantages offered by the implementation of new technologies in the wine agroindustrial sector to improve the conditions of the crops is deficient and little used, being that it is possible to detect external agents and anticipate risks that endanger the health of the entire plantation.

General objective

Generate an intuitive graphical interface capable of capturing and processing information of interest on the status of the crop from an analysis of discoloration or marbling of the leaf using color segmentation to generate a useful diagnosis for the user.

Particular objectives

- Generate a previous study of the object of study.
- Develop a graphical interface for data acquisition.
- Develop programming for information processing.
- Present expected results.

Diagnosis

The previous study is oriented to the design and construction of the system, considering a projective type research, using a descriptive method.

Wine sector

Viticulture is the science, technique and art of vine growing and grape production. (Pszczólkowski, 2007)

Disease Control

Cryptogamic diseases (caused by a fungus or other filamentous organism) of the vine such as powdery mildew, botrytis and mildew can be prevented by preventive applications of organic fungicides such as sulfur, citrus extracts, copper, compost tea, serum or biological fungicides. Among the cultural practices that can be used are leaf removal, grating and chapoda that are used to avoid favorable conditions for the development of diseases. (Torres, 2013)

Virus

The most important viruses that have been found in Spain are the infectious short internode (GFLV) and the coiled one (GLRV). In 1990 a study of virus-transmitting nematodes was carried out with the technical support of the hematology laboratory. Starting in 1992, diagnosis began using the E.L.I.S.A. test technique. the viruses of the short and coiled internode, thus confirming the suspicions raised (LÓPEZ, 1996).

Infectious short internode.

The virus that causes this disease belongs to the group called NEPOVIRUS. It is a virus that presents a wide picture of symptoms but that can be confused with characteristics of the variety, nutritional deficiencies, etc.

In leaves, it is observed that the petiolar sinuses are more open than in healthy strains, greater number of teeth and presence of nervous and yellow type mosaics (LÓPEZ, 1996).

Figure 2 Beige mosaic
Source: (LÓPEZ, 1996)

ISSN 2523-6776

Rolled up

The virus that causes this disease belongs to the group called CLOSTEROVIRUS.

In sheets, the edges are rolled down. These acquire a reddish coloration in the red varieties and in the white varieties a foliar yellowing is observed. (LÓPEZ, 1996).

Figure 3 Leaf curl and reddish coloration
Source: (LÓPEZ, 1996)

Based on the previous investigation carried out and consulting with personnel from the area, the different relevant characteristics were detected:

– Diseases in the vine.
– Pests
– Bacteria
– Virus.
– Mineral deficiency.

From the information obtained, the "leaf discoloration" of the plant is determined as the object of study of this work, which presents different characteristic features of the external agent that affects it.

Interface development.

Based on the information from the previous study, the interface is developed, contemplating providing it with particular characteristics that solve the problem and benefit the user in the best way.

As an initial proposal, a previous design of the graphical interface (Figure 4) is made that is intuitive and easy to use for the user; considering as the first stage the acquisition of the information in which the data corresponding to the captured image is stored for its subsequent filtering and processing using specialized techniques as part of the second stage and finally the interpretation and visualization of the results as the last stage.

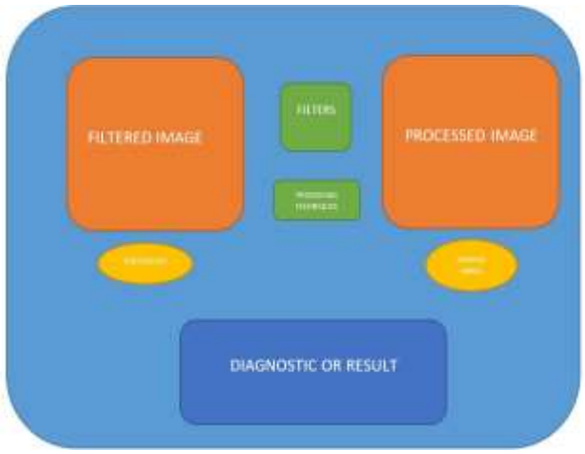

Figure 4 Proposal for the interface design
Source: Own Elaboration [Microsoft Word]

The interface is developed entirely in the MATLAB GUIDE environment, which integrates mathematical computation with visualization functions and a highly efficient language, offering a flexible means to carry out technical computation and taking advantage of the benefits offered by having a A wide variety of "toolbox" with a large number of built-in functions, facilitated the development of the program, reducing experimentation time and avoiding the need to interconnect codes between different programming languages (Figure 5).

Figure 5 Graphical User Interface (GUI)
Source: Own Elaboration [MATLAB]

ISSN 2523-6776

For the development of the GUI, it is considered that it complies with the proposed specifications and requirements, which is why it is divided into the following sections: image acquisition, information processing and diagnostic display, which are described below.

Image acquisition.

In this section the information corresponding to the images to be processed is captured (Figure 6). For this, the following elements are integrated:

- **Home button:** allows the user to initialize the camera power-on process.
- **Image capture button:** allows you to capture an image in real time using the camera.
- **Power off button:** when pressed, the camera turns off leaving a lock mode image.
- **Inset:** the function it gives us is to show the image in real time from the camera.

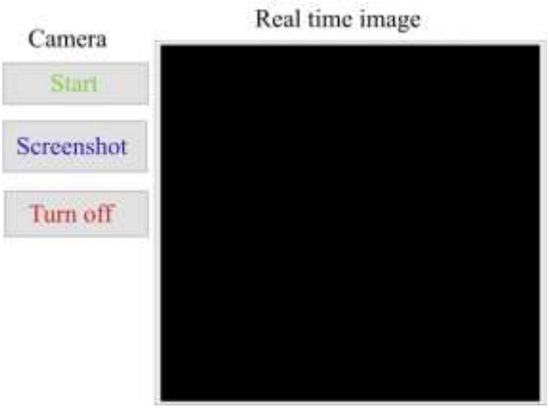

Figure 6 Image acquisition section
Fuente: Own Elaboration [MATLAB]

Information processing.

To store and process the information, the following elements are integrated (Figure 7):

- **Upload Image button:** allows you to choose an image stored as a file.
- **Inset:** displays the image captured by the camera or chosen from the computer when using the upload image button.
- **Filters:** allows you to select a variety of filters manually to better interpret the image.
- **Process button:** by pressing the button, an automatic color segmentation is carried out for the detection of patterns based on the discoloration of the object of study.
- **Clean button:** the action it performs is to delete the processed image and the information in general to be able to perform a new processing.

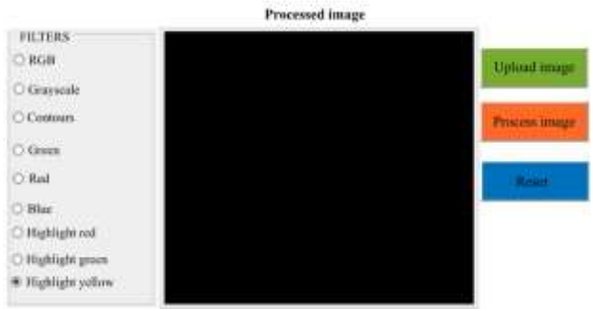

Figure 7 Information processing section
Source: Own Elaboration [MATLAB]

Diagnosis.

It allows us to visualize a diagnosis about the object studied in such a way that it is understandable for the user.

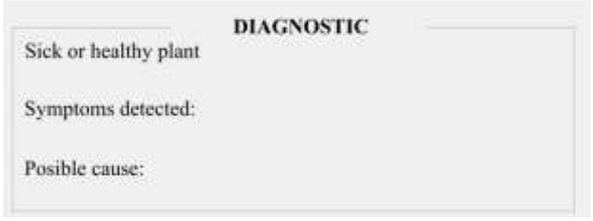

Figure 8 Diagnosis display section
Source: Own Elaboration [MATLAB]

Program development.

In this phase, the program was structured, combining the pre-built functions with written routines. Here are the sequences of the duties and the work they perform.

The initial part of the program is made up of the instructions to start the camera, capture images in real time, turn off the camera, and finally an instruction that allows the image to be viewed in real time.

The second part after acquiring the image is to pre-process it. The pre-processing stage is the application of techniques and tools to transform the image in order to improve it for subsequent processes.

ISSN 2523-6776

The first step in pre-processing is to make sure that the image contains the regions of interest in the best possible way. For this, the technique of applying filters was used to eliminate noise. There are numerous filters that apply pixel by pixel transformations, which not only depend on the hue of the pixel to be treated, but also on those of its neighbors. The application of these filters occurs through masks, square matrices with an odd number of rows. In the second and last step of the pre-processing, the binarization of the image was used, it is also a contrast enhancement technique. It is an extreme case, where the transfer function for dark and light tones is zero.

Subsequently, the fundamental step is carried out, which is to clearly differentiate all the elements that make up the image, this is achieved with a segmentation of images for this, a multitude of different processes and techniques can be applied, depending on the type of image and the desired result. Typically the segmentation of an image is based on the characteristics of shades of gray, such as discontinuity and similarity. Discontinuity searches for lines, edges, or points based on abrupt changes in the shade of gray, while similarity establishes regions based on the spatial or chromatic relationships that may exist between the pixels that form it.

The next step in recognition is the extraction of characteristics from the objects. This program extracts RGB color information from each object to later send an understandable diagnosis for the user.

All the above described functions were implemented in a graphical environment in order to create an interface that allows easy and comfortable execution of each of the different phases developed in the previous section. In addition, some data is collected and displayed that allow understanding the processing and proper interpretation of the results in said graphical interface.

Behind each interactive element that makes up the graphical interface is its corresponding function called callback. In this function the code that will have to be executed when interacting with the element is written, both the content of the buttons and the static texts and the titles of the panels, are previously configured in MATLAB.

Results

To generate the diagnosis, the information captured as an image of the study object is used in the space of the primary colors R-red, G-green, B-blue (RGB) (Figure 9).

Figure 9 Image to be processed RGB
Source: Own Elaboration [MATLAB]

Subsequently, the image processing is carried out by means of a visual inspection using filtering tools in the spatial domain to detect possible inconsistencies prior to performing the analysis by color segmentation (Figures 10 - 17).

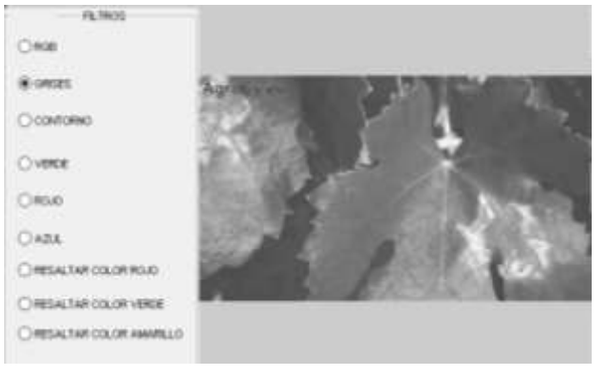

Figure 10 Image applying grayscale filter
Source: Own Elaboration [MATLAB]

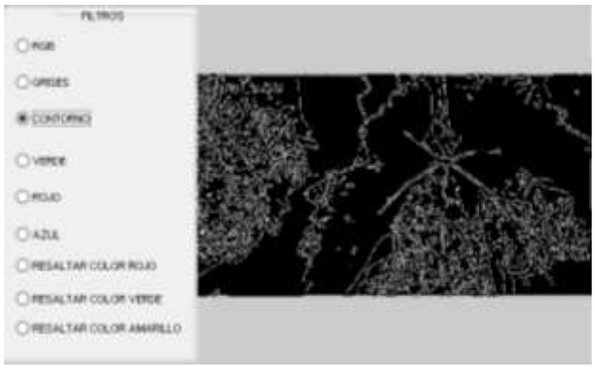

Figure 11 Image applying edge detection filter.
Source: Own Elaboration [MATLAB]

ISSN 2523-6776

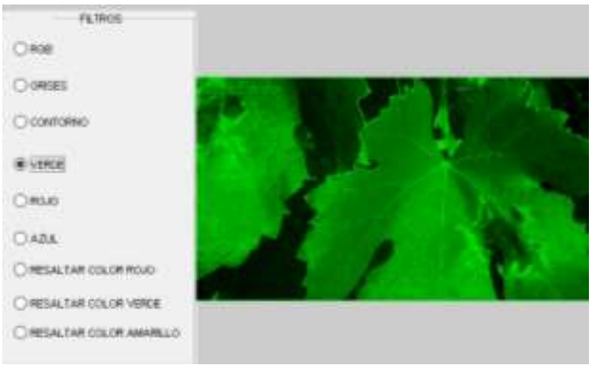

Figure 12 Image applying green filter
Source: Own Elaboration [MATLAB]

Figure 13 Image applying red filter
Source: Own Elaboration [MATLAB]

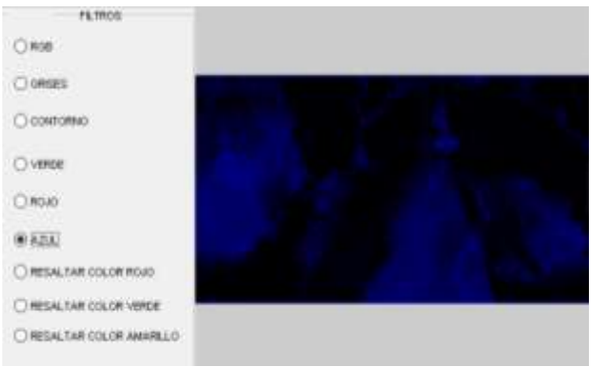

Figure 14 Image applying blue filter
Source: Own Elaboration [MATLAB]

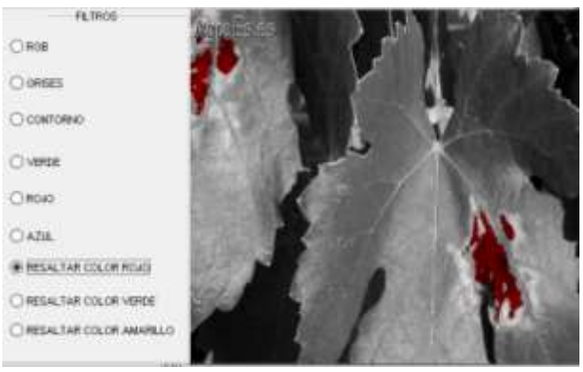

Figure 15 Image applying filter to highlight the red color
Source: Own Elaboration [MATLAB]

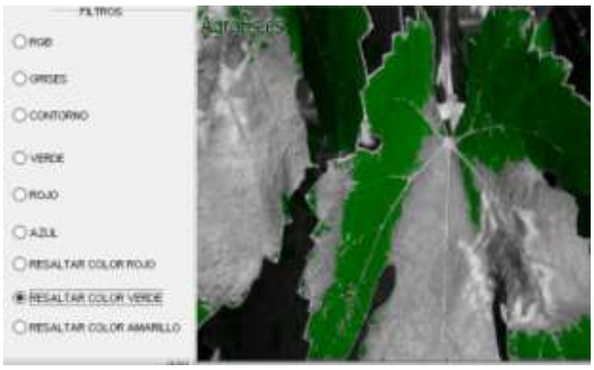

Figure 16 Image applying filter to highlight the green color
Source: Own Elaboration [MATLAB]

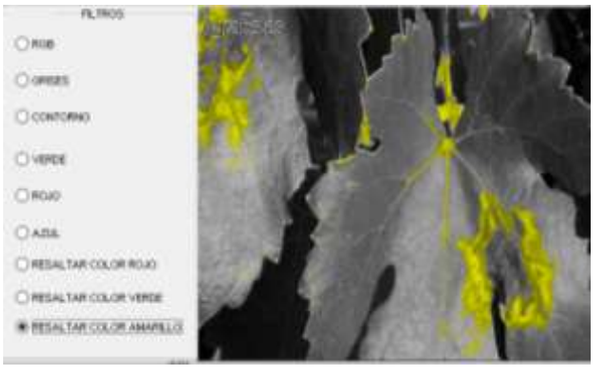

Figure 17 Image applying filter to highlight yellow color
Source: Own Elaboration [MATLAB]

Therefore, it is possible to generate a diagnosis from the detection of patterns by applying color segmentation tools using the graphical user interface. For this, samples with indications of marbling or discoloration on the sheet are analyzed.

In Figure 18, the captured image is processed to generate the diagnosis by detecting by color segmentation of the sections where yellowish mottling caused by a possible nutrient deficiency is present.

Figure 18 Nutrient deficiency diagnosis
Source: Own Elaboration [MATLAB]

ISSN 2523-6776

In Figure 19, the processing is performed from an image captured in file to generate the diagnosis by highlighting the detected sections where there is reddish mottling caused by a possible virus.

Figure 19 Virus Diagnosis
Source: Own Elaboration [MATLAB]

Conclusions

The analysis carried out in this research allowed obtaining relevant information about the object of study (vine leaf) and overcoming different challenges presented where a previous exploration was necessary to allow the correct assimilation of the data obtained and the interpretation of the results obtained.

With the development of this work, the first results were obtained, which will be very useful for later stages, so work will continue to implement new processing and pattern detection techniques that allow adjustments to be made to the results obtained and generate better diagnoses. that provide essential knowledge and tools for decision-making by users or producers.

References

Dobernack, N. A. (s.f.). *PROYECTO FIN DE CARRERA.* Recuperado el 18 de Agosto de 2021, de http://bibing.us.es/proyectos/abreproy/12112/fichero/Documento_por_capitulos%252F3_Cap%C3%ADtulo_3.pdf

Dueñas, C. P. (2009). *Introducción a la Visión.* Obtenido de http://www.ieef.upm.es/webantigua/spain/Asignaturas/MIP_VisionArtificial/ApuntesVA/cap1IntroVA.pdf

Grau, J. F. (2010). *Técnicas de análisis de imagen: Aplicaciones en Biología.* España: Universitat de valencia.

LÓPEZ, P. R. (1996). *PLAGAS Y ENFERMEDADES DE LA VID EN CANARIAS.* Canarias: GOBIERNO DE CANARIAS CONSEJERIA DE AGRICULTURA, GANADERÍA,PESCA Y ALIMENTACIÓN.

MathWorks. (Enero de 2020). *Descripción del producto MATLAB.* Obtenido de https://es.mathworks.com/help/matlab/learn_matlab/product-description.html

Moya, D. J. (26 de Mayo de 2012). *Procesamiento y Análisis de imagenes digitales* . Obtenido de http://www.ie.tec.ac.cr/palvarado/PAID/paid.pdf

Pszczólkowski, G. F. (2007). *Viticultura, Fundamentos para Optimizar Producción y Calidad.* Santiago, Chile: Universidad Católica de Chile.

Rivera, M. A. (2005). *El Diseño de Interfaz gráfica para cursos en línea* . Obtenido de https://arquitectura.unam.mx/uploads/8/1/1/0/81110907/2005-03-29260marr-ve2005.pdf

Torres, C. A. (2013). *Manual de VITIVINICULTURA ORGÁNICA.* Obtenido de https://www.socla.co/wp-content/uploads/2014/Manual-de-vitivinicultura-organica_pino.pdf

ISSN 2523-6776

Article **Journal of Technological Engineering**
June, 2021 Vol.5 No.15 9-16

Drag and lift force analysis for the cybertruck Tesla vehicle

Análisis de fuerzas de arrastre y sustentación para el vehículo Tesla Cybertruck

HORTELANO-CAPETILLO, Juan Gregorio[1]†*, MARTÍNEZ-VÁZQUEZ, J. Merced[1], BAÑOS-LOPEZ, Esperanza[2] and ALFARO-AYALA J. Arturo[3]

[1]*Universidad Politécnica de Juventino Rosas*
[2]*Universidad Autónoma del Estado de Hidalgo*
[3]*Universidad de Guanajuato*

ID 1st Author: *J. Gregorio, Hortelano-Capetillo* / **ORC ID**: 0000-0002-3702-4853

ID 1st Coauthor: *J. Merced, Martínez-Vázquez* / **ORC ID**: 0000-0002-6230-3846

ID 2nd Coauthor: *Esperanza, Baños-Lopez* / **ORC ID**: 0000-0003-3983-4507

ID 3rd Coauthor: *J. Arturo, Alfaro-Ayala* / **ORC ID**: 0000-0003-3081-282X

DOI: 10.35429/JTEN.2021.15.5.9.16 Received March 14, 2021; Accepted June 29, 2021

Abstract

In this research, aerodynamic tests were carried out at different speeds by using Solidworks Flow Simulation software in the Tesla Cybertruck vehicle, knowing the results of the drag and lift coefficients. The method was selected in three dimensions, the continuity equations and the Navier-Stokes equations that were solved by the finite volume method, the k-ε model was chosen to close the amounts of turbulence.

Drag coefficient, Lift coefficient, Aerodynamics

Resumen

En esta investigación se realizaron pruebas aerodinámicas a diferentes velocidades mediante el uso del software Solidworks Flow Simulation en el vehículo Tesla Cybertruck, conocer los resultados de los coeficientes de arrastre y sustentación. El método fue seleccionado en tres dimensiones, las ecuaciones de continuidad y las de Navier-Stokes que fueron resueltas por el método de volumen finito, el modelo k-ε fue elegido para cerrar las cantidades de turbulencia.

Coeficiente de arrastre, Coeficiente de sustentación, Aerodinámica

Citation: HORTELANO-CAPETILLO, Juan Gregorio, MARTÍNEZ-VÁZQUEZ, J. Merced, BAÑOS-LOPEZ, Esperanza and ALFARO-AYALA J. Arturo. Drag and lift force analysis for the cybertruck Tesla vehicle. Journal of Technological Engineering. 2021. 5-15: 9-16

* Correspondence to Author (e-mail: jhortelano_ptc@upjr.edu.mx)
† Researcher contributing as first author.

Introduction.

The Testa cybertruck shown in the Figure 1, was introduced in November 2019 that will be more useful than a traditional Pick-Up truck and will have a greater performance than a sport car, with a new class of resistance, speed, and versatility with a design fully electric. The powerful transmission and low center of gravity provide extraordinary traction and torque control. Allowing acceleration to go from 0 to 60 mph in just 2.9 seconds [1].

Figure 1 Tesla Cybertruck
Fuente: [1]

The first truck Pick-Up was built by brothers John and Horace Dodge during first world war under the name of Dodge Brothers [2], the first Chevrolet Pick-Up was called 490 Light Delivery with 4 cylinders of 21.7 Hp [3], Ford began to market its Pick-Up called Ford T Runabout [4]. Improving aerodynamics consists of reducing the drag and lift forces of a vehicle because it is related to fuel consumption.

A 1% reduction in the drag coefficient would equal a significant saving in fuel cost [4,5]. In terms of environtmental impact, the reduction of CO_2 emissions in recent decades has been one of the main objectives for the design of the most efficient vehicles. An estimated average with the most aerodynamic cas has a fuel saving of around 3-4% due to reduction in the drag coefficient of 10% [7,8]. Katz [9] and Regert et al. [10] proved that the drag force and the pressure distribution around the vehicle depend on the design and not on the friction of the surface.

The aerodynamics of Pick-Up trucks are more complex and have a coefficient of drag 15% higher than sport car and 25% higher than sedan vehicle [11]. Al-Garni et al. [12] observed that the coefficient of drag is high in a Pick-Up because of the complex interaction of the separate flow and the body, body walls, and tailgate that form a separate shear layer behind the cab. Holloway et al. [13] observed that the layer forms on the rear Pick-Up trucks, the Flow contains recirculating fluxes, unstable vortex shedding and other complex interactions.

All this phenomenon is of great interest for the aerodynamics of the truks, the losses at normal speed reach 60-70% of the total losses [14-16]. The drag force is the aerodynamic force that opposes movement, it is generated by the interaction and contact of a solid body with a fluid such as air. There are many factors that affect the magnitude of the drag force such as: the viscosity of the air and the viscous forces expressed to the movement such as the Reynolds number generating a flow limit layer along the solid surface [17]. The lift force is produced when cars travel at a high speed that causes the car to be unstable, this forcé is produced upwards. Therefore, the cars must be designed to reduce that lift force or implement some aerodynamic devices [17]. Figure 2 shows the different values of the drag coefficients (Cd) and lift (Cl) according to the shape and size for different aerodynamic profiles [18].

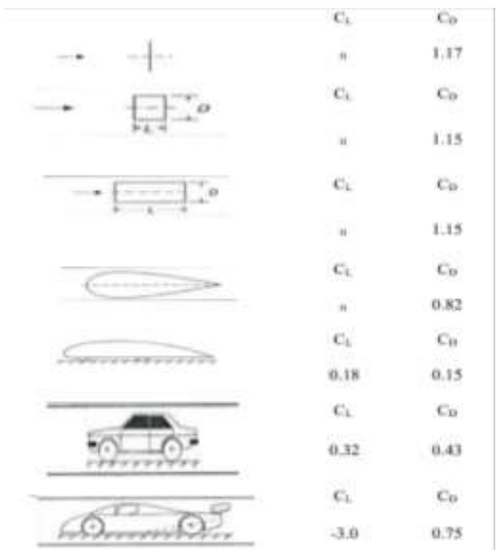

Figure 2 Drag (Cd) and lift (Cl) coefficients for different aerodynamic profiles [18]

ISSN 2523-6776

Figure 3 shows a comparison of the drag coefficients for different car models, a modern car achieves an average drag coefficient of 0.25-0.33 so that the aerodynamics obtain better performance.

In this research work, it will be demonstrated if the Tesla Cybertruck has excellent aerodynamics by calculating the drag and lift coefficients, later comparing it with data found in the literature as mentioned in Figure 3.

Mathematical and numerical model

CFD uses what is known as the finite element method, it is an approximation method used for solving fluid mechanics equations. Obtaining values of force, moments pressures, resistance to movement, etc., wich is the information obtained in a wind tunnel. In this work, several CFD tests were carried out to reproduce the aerodynamic behavior of the Tesla Cybertruck. Figure 4 shows the steps to solve a problem using CFD.

Car	Cx
Venturi VBB-3 (2013)	0,13
Volkswagen XL1 (2013)	0,189
Tesla Model S (2012)	0,24
Opel Insignia (2009)	0,27
Audi A3 (2003)	0,32
Audi A6 (1997)	0,28
Opel Kadett (1989)	0,38
BMW Serie 1 (2004)	0,31
Citroën CX (1974)	0,36
Citroën C4 coupe	0,28
Opel Astra (2004)	0,32
Peugeot 807 (2002)	0,33
Renault Espace (1997)	0,36
Renault Espace (2002)	0,35
Renault Vel Satis (2002)	0,33
Hispano Divo (2003)	0,349
Irizar PB (2002)	0,55

Figure 3 Drag coefficients (Cd) for different car designs [19]

- Geometry modeling: The first step is to design the parto or object that you want to study generated in CAD, for this case study, it is shown in Figure 5.
- Mesh generation: The CFD simulation is based on finite volumes, it is necessary to divide the model into small volumes, this known as meshing shown in Figure 7.
- Define models: In this step, the equations that the software will solve in the simulation are chosen continuity equation, Navier-Stokes equations, and turbulence models.
- Set properties: Define materials and their characteristics, fluids in the state they are, the air was selected for aerodynamic tests.
- Boundary conditions: The entry conditions must be specified, for this case different speeds were selected; and the boundary conditions the atmospheric pressure was selected.
- CFD simulations: Once the solid and the fluid have been perfectly selected, the simulation is carried out to obtain the convergence of the solution, the good behavior of the iterative process through residual diagrams.
- Results: Extract graphics, tables, videos, pressure contour, speed, temperature, streamlines, animations, etc.

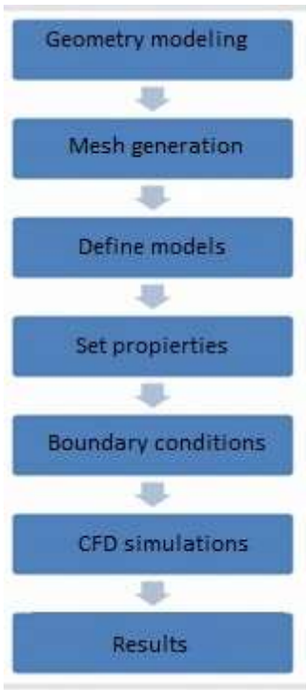

Figure 4 Steps for simulation in CFD
Source: Own Elaboration

The Tesla Cybertruk model is shown in Figures 5 and 6. Different views are observed, such as the front, side, rear, etc. The model was designed in Solidworks, later the aerodynamic simulations were carried out using the Flow Simulation plug-in. For an external aerodynamic analysis of a body, some coefficients must be considered, including the drag coefficient and the lift coefficient.

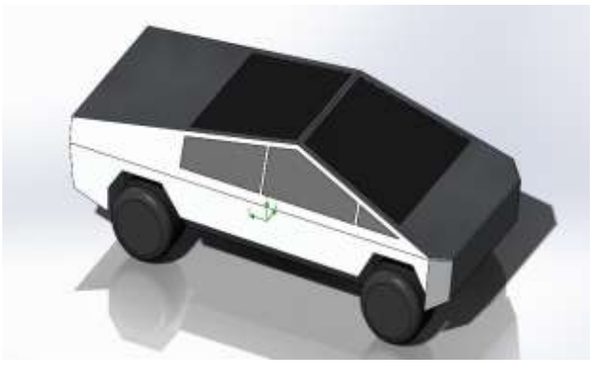

Figure 5 Design of the Tesla Cybertruck in Solidworks
Source: Own Elaboration

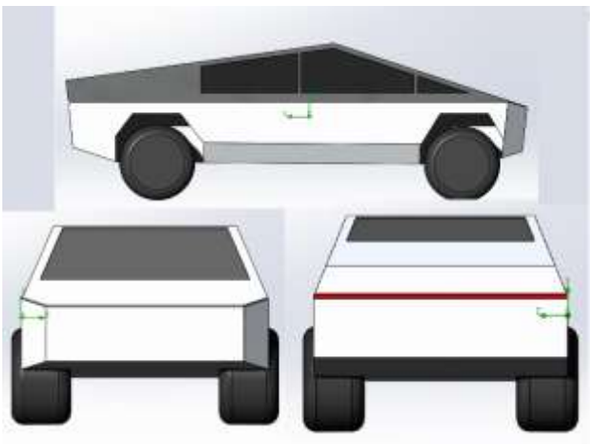

Figure 6 Design of Tesla Cybertruck in Solidworks, side, front, rear view
Source: Own Elaboration

Figure 7 show the control volume with 6043418 cells in the mesh made in Solidworks. The mesh is an important step for analysis in design, the software creates elements connected at points called nodes in Flow Simulation in hexahedral form, mesh control lets you specify different sizes of component elements, faces, edges, and vertices.The software creates a global element size for the model taking into account its volume, surface areas, and geometric details.

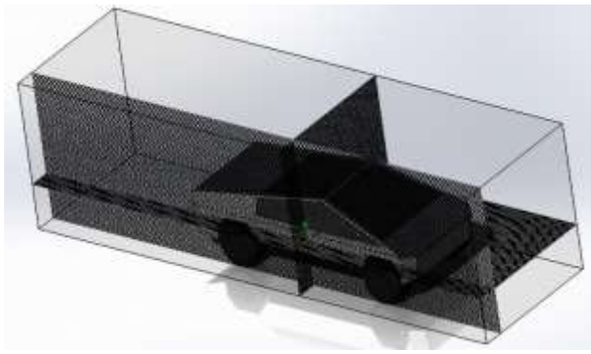

Figure 7 Control volume with 6043418 cells in the mesh
Source: Own Elaboration

Figure 8 shows the dimensions of the Tesla Cybertruck made in Solidworks in scale where it has a length of 1180 mm, height of 400 mm and width of 715mm.

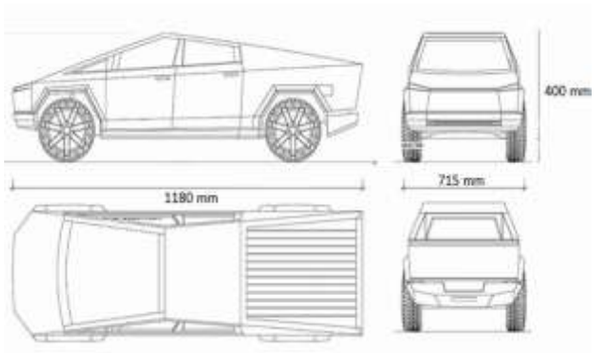

Figure 8. Tesla Cybertruck dimensions
Source: Own Elaboration

The aerodynamic study that presents the Flow developed around the vehicles requires a mathematical presentation, which in turn is transformed into an algorithm for its solution. This mathematical model is summarized in a set conservation equation of mass, momentum, and the turbulence model k-ε.

The continuity equation is represented by [20]:

$$\frac{\partial u}{\partial x}+\frac{\partial v}{\partial y}+\frac{\partial w}{\partial z}=0 \quad (1)$$

The Navier Stokes equations are expressed by [20]:

$$\rho\left(\frac{\partial u}{\partial t}+u\frac{\partial u}{\partial x}+v\frac{\partial u}{\partial y}+w\frac{\partial u}{\partial z}\right)=\rho g_x-\frac{\partial P}{\partial x}+\mu\left(\frac{\partial^2 u}{\partial x^2}+\frac{\partial^2 u}{\partial y^2}+\frac{\partial^2 u}{\partial z^2}\right) \quad (2)$$

ISSN 2523-6776

$$\rho\left(\frac{\partial v}{\partial t}+u\frac{\partial v}{\partial x}+v\frac{\partial v}{\partial y}+w\frac{\partial v}{\partial z}\right)=\rho g_y-\frac{\partial P}{\partial y}+\mu\left(\frac{\partial^2 v}{\partial x^2}+\frac{\partial^2 v}{\partial y^2}+\frac{\partial^2 v}{\partial z^2}\right) \quad (3)$$

$$\rho\left(\frac{\partial w}{\partial t}+u\frac{\partial w}{\partial x}+v\frac{\partial w}{\partial y}+w\frac{\partial w}{\partial z}\right)=\rho g_z-\frac{\partial P}{\partial z}+\mu\left(\frac{\partial^2 w}{\partial x^2}+\frac{\partial^2 w}{\partial y^2}+\frac{\partial^2 w}{\partial z^2}\right) \quad (4)$$

For turbulent flows the Standard *k*-ε model applies [21]:

$$\frac{\partial}{\partial t}(\rho k)+\frac{\partial}{\partial x_i}(\rho k u_i)=\frac{\partial}{\partial x_j}\left[\left(\mu+\frac{\mu_t}{\sigma_k}\right)\frac{\partial k}{\partial x_j}\right]+G_k+G_b-\rho\varepsilon-Y_m+S_k \quad (5)$$

$$\frac{\partial}{\partial t}(\rho\varepsilon)+\frac{\partial}{\partial x_i}(\rho\varepsilon u_i)=\frac{\partial}{\partial x_j}\left[\left(\mu+\frac{\mu_t}{\sigma_\varepsilon}\right)\frac{\partial \varepsilon}{\partial x_j}\right]+C_{1\varepsilon}\frac{\varepsilon}{k}(G_k+C_{3\varepsilon}G_b)-C_{2\varepsilon}\rho\frac{\varepsilon^2}{k}+S_\varepsilon$$

In these equations, G_k represents the generation of turbulence kinetic energy due to average velocity gradients. G_b is the generation of turbulent kinetic energy due to flotation. Y_m represents the contribution of fluctuating dilation in compressible turbulence for all dissipation rates. $C_{1\varepsilon}$, $C_{2\varepsilon}$ and $C_{3\varepsilon}$ are constant. σ_k and σ_ε are the turbulent Prantl numbers for *k* and ε respectively. S_k y S_ε are user defined source terms. Turbulent viscosity μ_t is calculated by:

$$\mu_t=\rho C_\mu\frac{k^2}{\varepsilon} \quad (6)$$

The parameters of some constants are:

$C_{1\varepsilon}$=1.44, $C_{2\varepsilon}$=1.92, C_μ=0.09, σ_k=1.0, σ_ε=1.3

To calculate the drag coefficient, equation (7) is used, where F_x is the drag force (N), ρ is the air density (kg/m^3), v is the air speed (m/s) and A is the front area of the car [20], for this study the area is 0.286 m^2.

$$Cd=\frac{Fx}{(1/2)\rho v^2 A} \quad (7)$$

The lift force as perceived from its inception is normal to the ground. Equation (8) shows the calculation of the lift coefficient, where F_y is the lift force:

$$Cl=\frac{Fy}{(1/2)\rho v^2 A} \quad (8)$$

Fort he análisis of this work, air is used at speed of 80, 100, 120, 140, 160, 175, 200, 225 and 250 km/h with a mesh number of 6043418, the density of air is 1.2 kg/m^3 and the viscosity 1.8x10^{-5} Pa.s.

With the results of the simulations, it is intended to know the drag and lift forces, later to calculate the coefficients to know the best aerodynamic model with the spoiler implemented in the rear that reduces these forces compared to normal models.

Results

Figure 9 shows the results of the drag forces (F_x) and lift (F_y) at speeds of 80, 100, 120, 140, 160, 175, 200, 225 and 250 km/h obtained through simulations in Solidworks, it is observed that the results of the forces increase as the speed increase.

Once the drag and lift force were obtained, the drag a lift coefficient shown in Figure 10 were calculated, it is observed that the drag coefficient has a range of 0.22-0.227 and the lift coefficient of 0.11-0.117 at different speeds. Therefore, the coefficients remain constant when the speed is increasing.

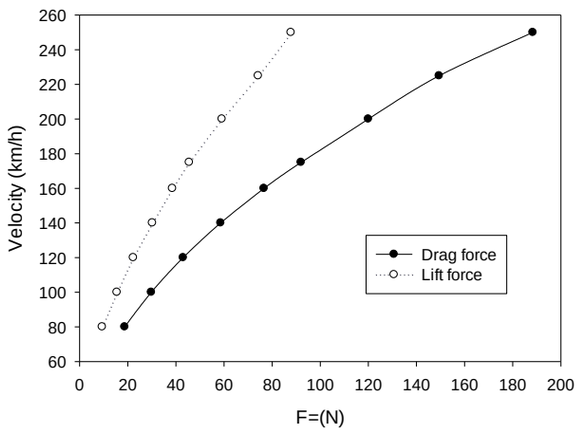

Figure 9 Results of the drag and lift forces obtained in Solidworks simulation
Source: Own Elaboration

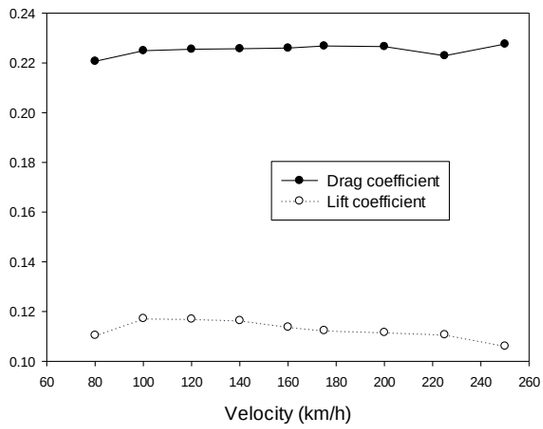

Figure 10 Results of the drag and lift coefficients obtained in Solidworks simulation
Source: Own Elaboration

Figure 11 shows the pressure contours on the outside of the Tesla. It is observed that the highest pressure by the wind is in the front part (color rojo) with a value of 102051.95 Pa (1.02 bar) and the lowest pressure is 100087.09 Pa (1 bar) at speed of 250 km/h.

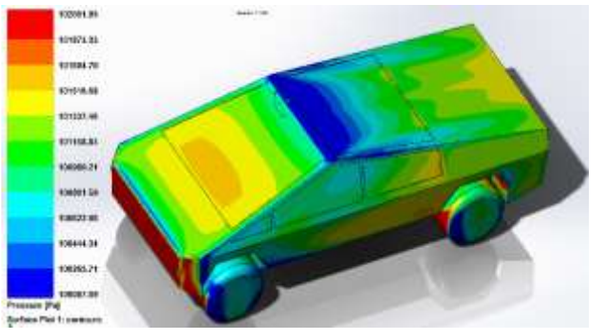

Figure 11 Results of the pressure contours at speed of 250 km/h obtained in Solidworks simulation
Source: Own Elaboration

The speed contours are shown in Figure 12 simulated at the speed of 250 km/h; it is observed that in the rear part the wake of vortices is formed with low speeds that cause the pressure to decrease.

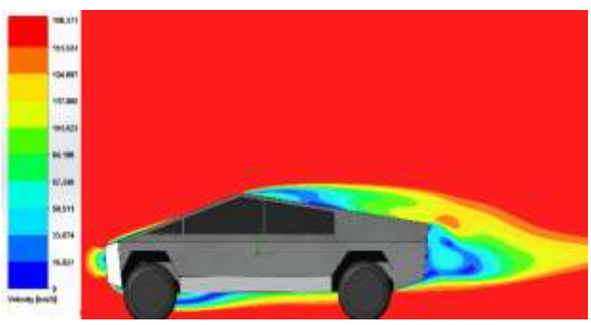

Figure 12 Results of the speed contours obtained in Solidworks simulation
Source: Own Elaboration

The following figures show the contours at different speeds. Figure 13 shows contours at the speed of 80 km/h, Figure 14 contours de speed at 120 km/h, Figure 15 contours of speed at 180 km/h and Figure 16 contours of speed at 250 km/h.

As the speed increases, the contours increase due to the turbulence generated in the rear part, this phenomenon is very important because the drag and lift force decrease due to the detachment of the boundary layer.

Figure 13 Results of the speed contours at 80 km/h obtained in Solidworks
Source: Own Elaboration

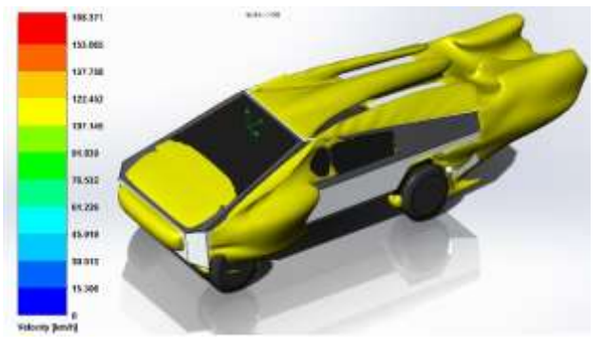

Figure 14 Results of the speed contours at 120 km/h obtained in Solidworks
Source: Own Elaboration

Figure 15 Results of the speed contours at 180 km/h obtained in Solidworks
Source: Own Elaboration

ISSN 2523-6776

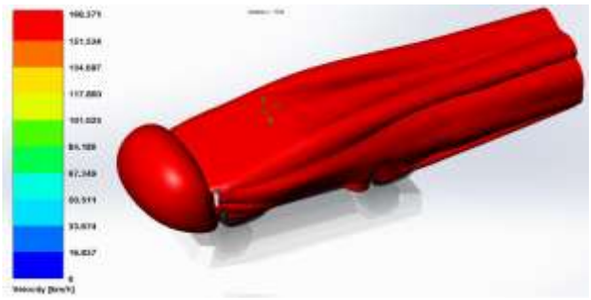

Figure 16 *Results of the speed contours 250 km/h obtained in Solidworks*
Source: Own Elaboration

Conclusions

Making a comparison of the results of the drag coefficient of the Tesla Cybertruck and data of some cars shown in Figure 3, it is concluded that the Tesla car has a design that guarantees excellent aerodynamic results with an average drag coefficient in a range of 0.3-0.4, the Tesla model S (2012) has a drag coefficient of 0.24 and 0.189 for the Volkswagen.

The results of the lift coefficient were obtained an average of 0.11, a very low coefficient that guarantees the stability of the Tesla. On the part of the computer equipment, while the mesh is finer the longer it will take to solve the simulation and the results will be more exact to reality depending on the characteristics of the computer.

Referencias.

[1] https://www.tesla.com/es_MX/cybertruck

[2] Sisson, Richard. 2007. *The American Midwest: An Interpretive Encyclopedia*. Ed. Indiana University Press, 1a edition, pp. 1423-1424.

[3] Gunnell, John., 2003. *Standard Catalog of Chevrolet 1912-2003*. Ed. Krause Publications, 3a edition, pp. 12-13.

[4] Gunnell, John., 2008. *Standard Catalog of Ford*. Ed. Krause Publications, 1a edition, pp. 12.

[5] Mohamed-Kassim Z., Filippone A., 2010. *Fuel savings on a heavy vehicle via aerodynamic drag reduction.* Transportation Research Part D: Transport and Environment. 15 (5), pp. 275-284.

[6] Paolo F., 2009. *The effect of the competition between cars and trucks on the evolution of the motorway transport system.* Transportation Research Part C: Emerging Technologies, 17 (6), pp. 558-570.

[7] Cooper K. R., 2004. *Commercial vehicle aerodynamic drag reduction: historical perspective as a guide.* In: The Aerodynamics of Heavy Vehicles: Trucks, Buses and Trains. Springer, Berlin, Heidelberg, pp. 9-28.

[8] Sovran G., 1983. *Tractive-energy-based formulae for the impact of aerodynamics on fuel economy over the EPA driving schedules.* No. 830304. SAE Technical Paper.

[9] Katz J., 2006. Aerodynamics of race cars. Annu. Rev. Fluid Mech. 38. Pp. 27-63.

[10] Yang Z., Khalighi B., 2005. *CFD simulations for flow over Pickup trucks.* SAE Paper No. 2005-01-0547.

[11] Al-Garni A., Bernal L., Khallghi B., 2003. *Experimental investigation of the near wake of a Pickup truck.* In: SAE World Congress, 2004-01-0228, Detroit, USA.

[12] Holloway S., Leylek J. H., York W. D., Khaligui B., 2009. *Aerodynamics of a Pickup truck: combined CFD and experimental study.* SAE Int. Journal Commercial Vehicles 2, pp. 88-100.

[13] Roshko A., 1993. *Perspectives on bluff body aerodynamics.* Journal Wind Engineering Industrial Aerodynamic. 49. pp. 79-100.

[14] Choi H., Lee J., Park H., 2014. *Aerodynamics of heavy vehicles.* Annu. Rev. Fluid Mech. 46. pp. 441-468.

[15] Schuetz T. C., 2015. *Aerodynamics of road Vehicles.* Fifth ed. SAE International.

[16] R. B. Bird., (1992). Fenomenos de Transporte. Editorial Reverte. Barcelona España.

[18] Hucho W. H., Gilhaus A., Hoffman., (1998). *Aerodynamics of a road vehicle*. USA: SAE International.

ISSN 2523-6776

[19] https://es.paperblog.com/la-resistencia-aerodinamica-y-el-coeficiente-cx-en-el-automovil-4678075/

[20] Robert W. Fox., Alan T. MacDonald., Philip J. Pritchard., 2003. Introduction to Fluid Mechanics, Sixth Edition.

[21] V. Yakhot., L. M. Smith., 1992. *The renormalization group, the ε-expansion and derivation of turbulence models.* Journal of Scientific Computing, Vol. 7, no. 1, pp. 35-61.

ISSN 2523-6776

Article **Journal of Technological Engineering**
June, 2021 Vol.5 No.15 17-35

Direct design process of aerodynamic profiles using the Joukowsky transformation

Proceso de diseño directo de perfiles aerodinámicos mediante la transformación de Joukowsky

ROMERO-GÓMEZ, Gabriel Adrián†* & LÓPEZ-GARZA, Víctor

Universidad Michoacana de San Nicolás de Hidalgo, Facultad de Ingeniería Mecánica. Ciudad Universitaria, Colonia Felicitas del Rio 58060 Morelia, México.

ID 1st Author *Gabriel Adrián, Romero-Gómez* / **ORC ID:** 0000-0001-7841-8472

ID 1st Co-autor: *Víctor, López-Garza* / **ORC ID:** 0000-0001-9090-9119, **Researcher ID Thomson:** H-6969-2018, **Open ID:** 10747067300784159738 2, **CVU CONACYT ID:** 55431

DOI: 10.35429/JTEN.2021.15.5.17.35 Received March 14, 2021; Accepted June 29, 2021

Abstract

This document shows the results of a part of the direct design process of airfoils. The research and design of these geometric shapes are of great relevance for their application in aerodynamic devices, since, if a wing profile with a great aerodynamic fineness is developed, the efficiency of the devices that have this geometric shape will be improved on its wings, propellers, etc. This project started from two analytical processes, the first was to obtain the shape of the wing profiles through the Joukowsky transformation, later the pressure distribution of each aerodynamic profile was obtained through the methodology developed by Theodorsen, the profiles that achieved optimal results were subjected to the third and last analysis in the Qblade software, this software allows to find the angle of attack that produces the maximum aerodynamic fineness, in addition to an approximation to the lift and drag coefficients, in this way several curved and aerodynamic profiles were obtained. Various thicknesses whose aerodynamic fines range between 100 and 250 at the optimum angle of attack.

Aerodynamic Fineness, Direct design process, Joukowsky transformation, Theodorsen methodology

Resumen

Este documento muestra los resultados de una parte del proceso de diseño directo de un perfil alar. La investigación y el diseño de estas formas geométricas son de gran relevancia para su aplicación en dispositivos aerodinámicos, ya que, si se llega a desarrollar un perfil alar con una gran fineza aerodinámica, se mejorará la eficiencia de los dispositivos que cuente con estaforma geométrica en sus alas, hélices, etc. Este proyecto partió de dos procesos analíticos, el primero fue obtener la forma de los perfiles alares a través de la transformación de Joukowsky, posteriormente se obtuvo la distribución de presiones de cada perfil aerodinámico mediante la metodología desarrollada por Theodorsen, algunos de perfiles que consiguieron resultados óptimos fueron sometidos al tercer y último análisis en el software Qblade, este software permite encontrar el ángulo de ataque que produce la máxima fineza aerodinámica, además de una aproximación a los coeficientes de sustentación y arrastre, de esta forma se obtuvieron varios perfiles aerodinámicos curvos y de diversos espesores cuyas finezas aerodinámicas oscilan entre 100 y 250 en el ángulo de ataque óptimo.

Fineza aerodinámica, Proceso de diseño directo, Transformación de Joukowsky, Metodología de Theodorsen

Citation: ROMERO-GÓMEZ, Gabriel Adrián & LÓPEZ-GARZA, Víctor. Direct design process of aerodynamic profiles using the Joukowsky transformation. Journal of Technological Engineering. 2021. 5-15: 17-35

* Correspondence to Author (e-mail: grog160998@gmail.com)
† Researcher contributing as first author.

Introduction

The design process of an aerodynamic profile or aerodynamic profile is usually complex, since these geometries must be applied to the cross-sections of the wings that will perform the task of supporting any aircraft in the air, this in the particular case of aerial vehicles. Aerodynamic profiles intended for subsonic aircraft generally have a great thickness in their geometry necessary to facilitate the generation of the force that sustains said aircraft in the air [2] pp. 92-93, however, due to the thickness of the wing profile, the amount of air hitting the airfoil is greater and consequently the drag force increases.

The drag force is that dynamic effect that opposes the displacement of the aircraft in the sky and this impairs the efficiency of the aerodynamic profile, this means that a profile whose thickness is less will generate less lift and drag compared to another medium or thick thickness, although a different way of increasing the support force without increasing the thickness of the profile is by generating a curvature in the trajectory of the profile contour, so the objective of the design of aerodynamic profiles in the present work was to obtain aerodynamic curves profiles, this To obtain specimens whose aerodynamic fineness is the highest possible, said fineness is the relationship between lift and drag force.

For the design of the aerodynamic profiles, a direct design process was used, which consists in that, based on the geometry of the wing profile, its aerodynamic properties are quantified and according to the results of the analysis it is decided if the profile is suitable for application. The geometries were obtained through an analytical process, this method is the result of a transformation of complex numbers known as conformal transformation, said transformation was carried out by the mechanical engineer Nikolái Yegórovich Joukowsky, for this reason this method was named in his honor as the Joukowsky transformation. The next step, after obtaining the geometries of the wing profiles, through the conformal transformation, was to study the profiles using the methodology developed by Theodorsen, this being the first approximation in our research project to the velocity and pressure distributions of the profiles.

Based on the results obtained, only those profiles whose pressure distributions were convenient for the research objective were selected, after the above, the selected profiles were studied in the Qblade software, thus obtaining profiles with a coefficient relationship of lift with respect to the drag coefficient up to 250. The hypothesis is that the profiles can develop better lift coefficients by introducing in them an adequate curvature in the geometry of the aerodynamic profile.

We will divide the present work into three sections, the first one quickly deals with what the Joukowsky transformation is, as well as showing the graphs of the profiles plotted in the Matlab software; the second section shows the pressure distributions in the aerodynamic profiles resulting from the Theodorsen method; and finally, the third section shows the results obtained in the Qblade software.

1. Profiles obtained by the Joukowsky transformation.

The Joukowsky transformation is a type of complex point-to-point transformation that allows transforming a region of complex numbers to another pre-established by the first and also preserving the angles of the original region, due to the aforementioned properties, this type of transformation is called as conformal transformation. Joukowsky, using the parametric equation of the circumference and a suitable conformal transformation, managed to develop a methodology to achieve wing profile geometries.

According to [3], p. 129, the Joukowsky transformation is defined as follows.

$$Y = f + \frac{C^2}{16f} \tag{1}$$

The variable $"Y"$ symbolizes the complex function that represents the points in the transformed plane that has the shape of the aerodynamic profile, $"f"$ is another complex function that describes the points of the closed curve of the circumference and the constant $"\frac{C^2}{16}"$ is equal to the coordinate on the axis of the real numbers where the transformation is not conforming.

For the complex transformation, in the coordinate of the circumference, to be conformal, this coordinate must comply with the first theorem of the conformal mapping.

"If f (z) is analytical and f´ (z) ≠ 0 in a region R, then the transformation w = f (z) is conformal at all points of R" Spiegel et al., (1991), cited by [5].

To simplify the transformation in the present work, this formula was manipulated to express it mathematically as follows.

$$z' = z + \frac{b^2}{z} \quad (2)$$

The letter "z" corresponds to the complex analytical function of the first region that represents the curve of the circumference, and its equation is the following.

$$z = -b + a\,(e^{i\beta} + e^{it}) \quad (3)$$

The complex variable "z´" is the corresponding curve that describes the wing profile, while "b", "a", "β" and "t" are the point of the trailing edge or the coordinate where the transformation does not it conforms due to the abrupt change in the angle tangent to the curve, the radius of the circumference, the angle of elevation of the circumference, and the variable whose range goes from zero to twice pi. The following figures show the parameters in better detail.

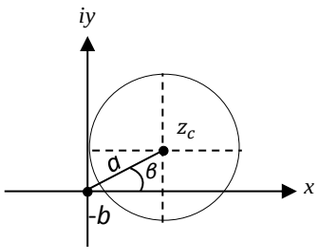

Figure 1.1 Established region of the variable "*z*"

In Figure 1.1 you can see the closed curve that describes the complex analytical function "z", in addition, the parameters "b", "a" and "β" are indicated, which define the position and radius of the circumference, in addition, "z_c" is the coordinate of the center of the circle.

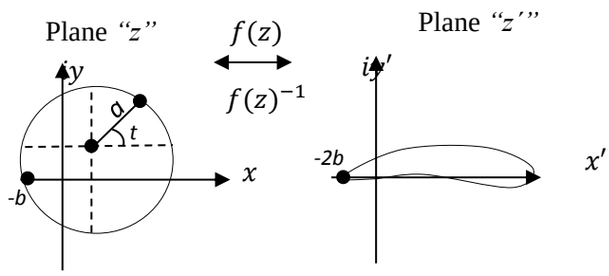

Figure 1.2 "z" and "z´" planes

Figure 1.2 shows the "z" plane and the transformed "z´" plane, the two-way arrow indicates that the process is reversible, that is, from a circumference through the transformation as an aerodynamic profile can be obtained and vice versa. The larger the ratio between "b" and "a", the thinner the profile. It should be noted that this ratio should not exceed one and the greater the magnitude of "β" the profile will have a more pronounced curvature, however, it is recommended that this value does not exceed ten degrees.

From this transformation, the coordinates of the curves of the wing profiles were obtained, whose geometric properties are reflected in the nomenclature that was implemented. First in the nomenclature, it is written in capital letter *"R"* which refers to the relationship between "b" and *"a"* and next to this its value, later it is written, in the same way, in capital letter *"B"* which makes reference to the magnitude in sexagesimal degrees of the beta parameter and, as the last data, *"A"* that indicates the degree of inclination of the profile with respect to the horizontal axis which was plotted, that is, its angle of attack.

Table 1.1 lists the profiles developed through the Joukowsky transformation, in addition to including the maximum thickness in percentage of the chord of the profile, the position of the maximum thickness in percentage of the chord, the maximum curvature and the position of the maximum curvature in percentage of the chord or also called the maximum ordinate. Next, it is shown, from Figure 1.3 to Figure 1.7, the geometries of the aerodynamic profiles listed in Table 1.1.

Aerodynamic profile code	Maximum thickness in percentage of the rope.	Maximum chord thickness position in percent
R0.9B5A0	12.55	24.7
R0.95B5A0	6.02	24.2
R0.85B10A0	18.13	24.4
R0.87B10A0	15.51	23.5
R0.9B10A0	11.35	24.48
R0.92B10A0	8.78	24.49
Aerodynamic profile code	**Maximum curvature**	**Maximum ordinate in percent of the chord.**
R0.9B5A0	4.35	50.5
R0.95B5A0	4.37	48.5
R0.85B10A0	8.24	50.8
R0.87B10A0	8.29	52
R0.9B10A0	8.82	49.28
R0.92B10A0	8.82	50.09

Table 1.1 List of profiles obtained by Joukowsky transformation

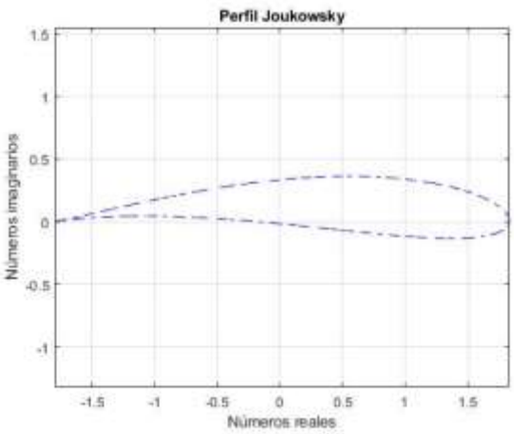

Figure 1.3 Profile R0.9B5A0

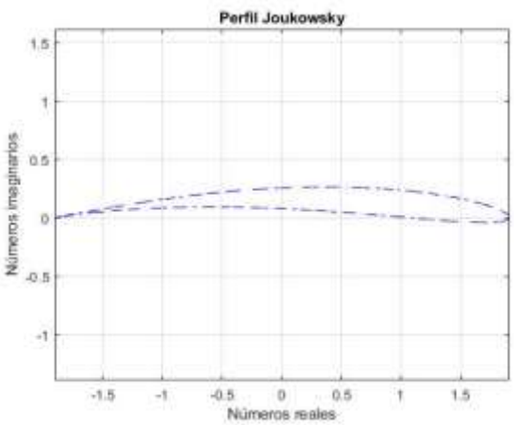

Figure 1.4 Profile R0.95B5A0

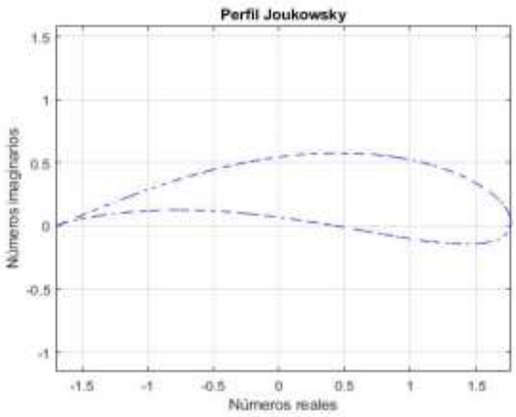

Figure 1.5 Profile R0.85B10A0

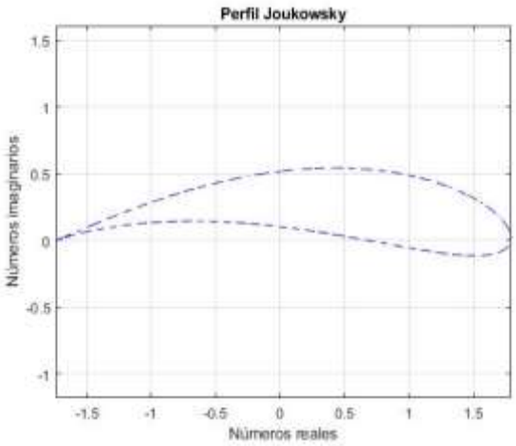

Figure 1.6 Profile R0.87B10A0

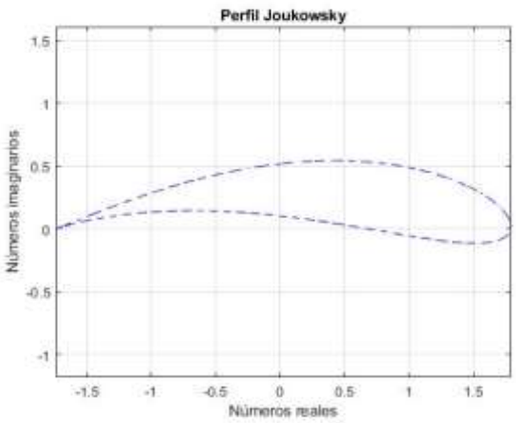

Figure 1.7 Profile R0.9B10A0

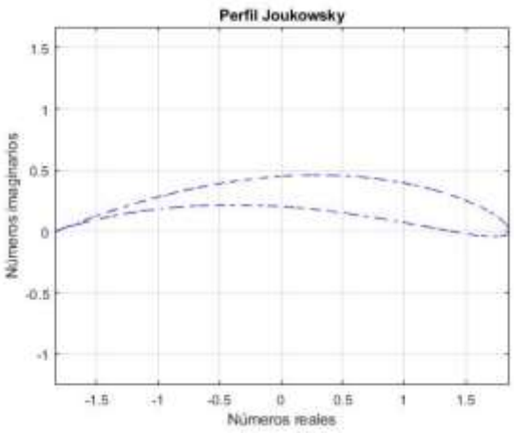

Figure 1.8 Profile R0.92B10A0

2. Theodorsen method

It has been shown that the potential flow field of a cylinder can be related to a potential flow of an airfoil by conformal transformation. Theodorsen implemented, through the relationship, a methodology in an analytical way to obtain the pressure and velocity distribution of the streamlines that circulate around any aerodynamic profile. This methodology was obtained from [5].

The results obtained were for the profiles located in Table 1.1, at an angle of attack identical to zero, this because the aerodynamic fineness tends to increase when the angle of attack increases, therefore, if the profile generates a satisfactory distribution when those airfoils are in a horizontal position, this distribution improves as the angle of attack increases. The result of this methodology is only an approximation to the real effects caused by the flow, since the analysis is carried out under the assumptions of incompressible air, ideal fluid and irrotational flow.

Next, the graphs of the distributions of the pressure coefficient, corresponding to the vertical axis, with respect to the percentage of the chord of each one of the profiles, corresponding to the horizontal axis, are presented; Figure 2.1, Figure 2.2, Figure 2.3, Figure 2.4, Figure 2.5 and Figure 2.6.

The results of the coefficient of pressure around the airfoil were used to calculate the coefficient of lift using the following formula.

$$Cl = \int_{Li}^{Ls} \left[\frac{Cp(x)_{Extrados} - Cp(x)_{Intrados}}{Ls - Li} \right] dx \quad (4)$$

The difference "Ls - Li" represents the chord of the aerodynamic profile and "$Cp\ (x)\ Extrados$" the local pressure coefficient in each of the coordinates along the chord of the profile on the extrados as a function of $"x"$, while "$Cp\ (x)\ Intrados$" is the local pressure coefficient in the intrados as a function of $"x"$. The integration was applied for each of the profiles. Graph 2.1 shows the lift coefficient of each of the aerodynamic profiles based on equation number four and the results obtained using Theodorsen's method.

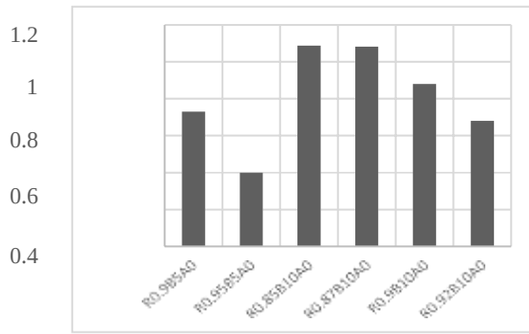

Graph 2.1 Support coefficients of the profiles

In Graph 2.1 the R0.9B5A0 profile was the geometry that generated the lowest lift coefficient of all the aerodynamic profiles. This result was already expected since the pressure distribution of the profile was obtained, which is represented in Figure 2.2, however, its study continued because it is the thinnest profile of the six, and that, due to its little thickness, the drag coefficient was expected to be much less than its lift coefficient. Another equation deduced by William Kutta and Joukowsky was the equation that calculates the circulation generated by an aerodynamic profile, mathematically it is expressed as follows.

$$\Gamma = 4\pi U_{\infty} a Sen(\alpha \pm \beta) \quad (5)$$

Substituting the circulation equation, equation (5), with respect to the Kutta-Joukowsky theorem equation, a mathematical formula is obtained capable of calculating the lift force of a wing profile.

$$L = 4\pi\rho {U_{\infty}}^2 a Sen(\alpha \pm \beta) \quad (6)$$

Therefore, assuming that the surface of the wing profile is equal to twice the radius of the circumference of the foreground, the lift coefficient will be as follows.

$$CL = 2\pi Sen(\alpha \pm \beta) \quad (7)$$

"Γ" is the flow generated by the aerodynamic profile, "U_∞" is the speed of the free stream, "a" is the radius of the circumference, "α" is the angle of attack and "β" is the angle of elevation. of the circumference.

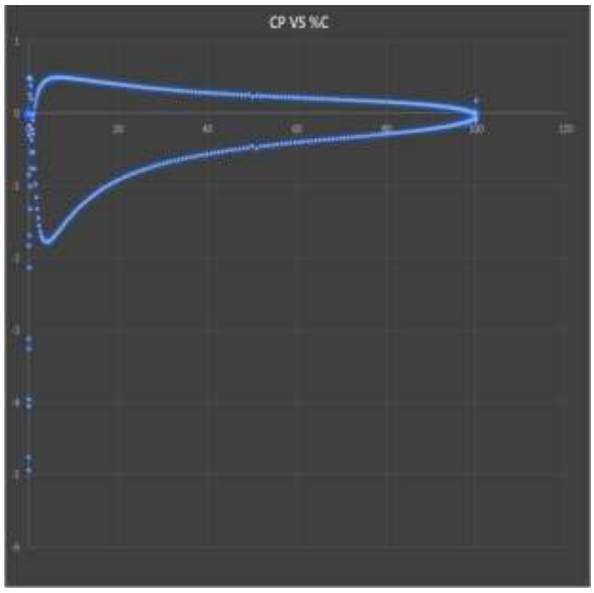

Figure 2.1 Pressure distribution of profile R0.9B5A0

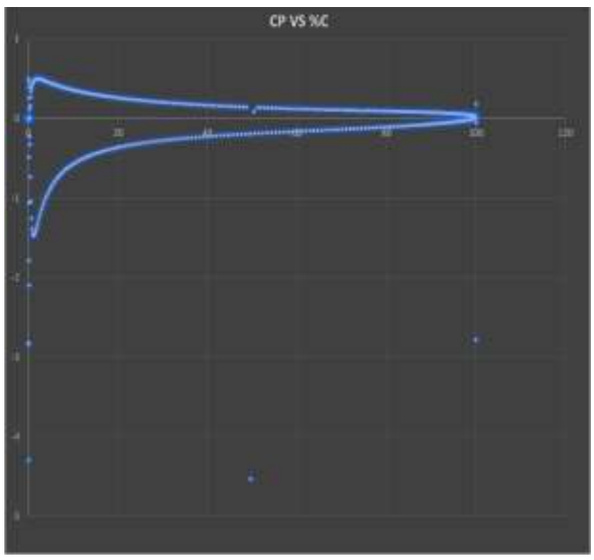

Figure 2.2 Pressure distribution of profile R0.95B5A0

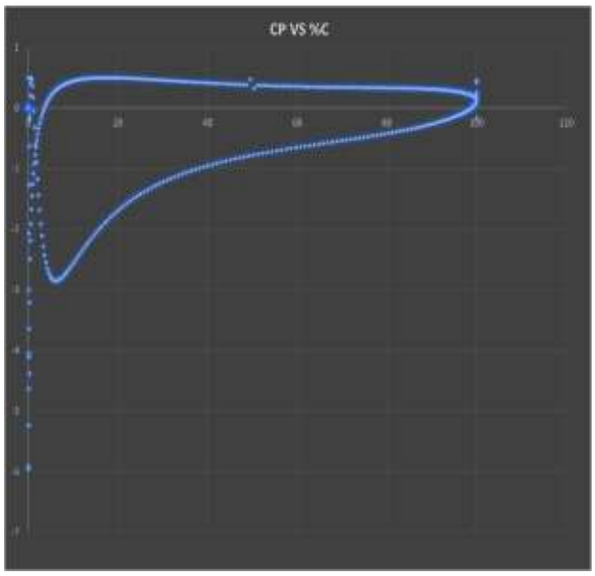

Figure 2.3 Pressure distribution of profile R0.85B10A0

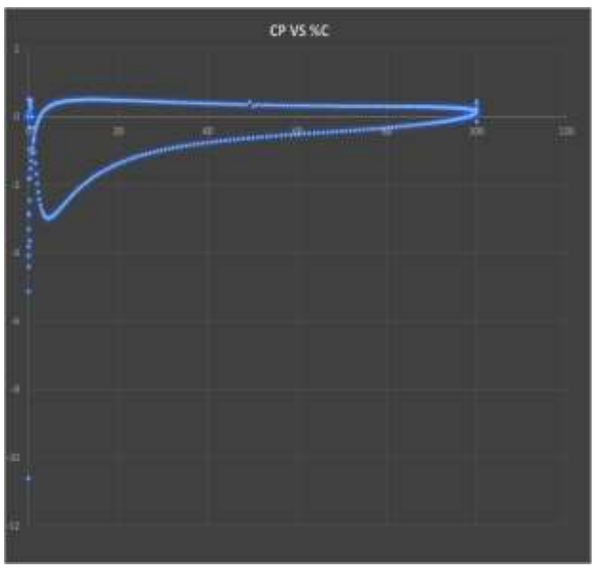

Figure 2.4 Pressure distribution of profile R0.87B10A0

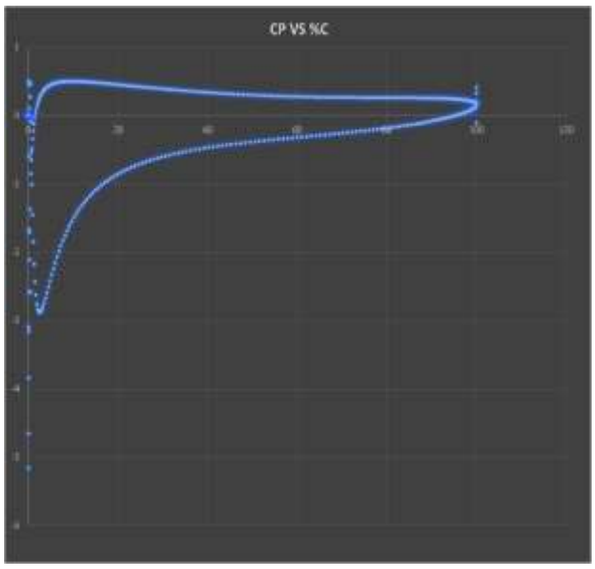

Figure 2.5 Pressure distribution of profile R0.9B10A

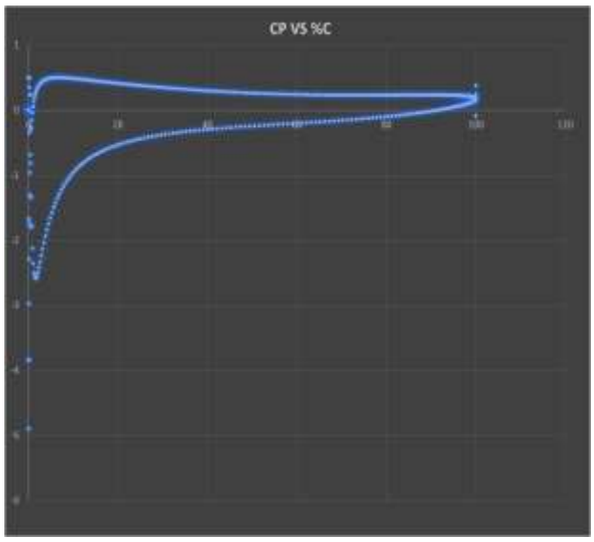

Figure 2.6 Pressure distribution of profile R0.92B10A0

Comparing the results obtained, it was observed that different results are obtained between both methodologies. The aerodynamic profile shown in Figure 1.3, is a profile of medium thickness, the generation of the pressure coefficients is satisfactory, according to the Theodorsen method the lift coefficient "Cl" is 0.73, this value is close to the value of the coefficient lift of 0.54, from equation (7), however, the deviation between the two values is -25% with respect to the Theodorsen method. The approximation has a substantial difference with respect to the method developed by Theodorsen, being, in this case, the different results due to the thickness of the profile.

The aerodynamic profile shown in Figure 1.4, is a thin thickness profile, the generation of the pressure coefficients is satisfactory, according to the Theodorsen method the lift coefficient "Cl" is 0.4, this value is close to the value of the coefficient lift of 0.54, from equation (7), however, the deviation between the two values is 35% with respect to Theodorsen's method. The approximation has a substantial difference with respect to the method developed by Theodorsen, being, in this case, the different results due to the thickness of the profile.

The aerodynamic profile, shown in Figure 1.5, is a thick thickness profile, the generation of the pressure coefficients is satisfactory, according to the Theodorsen method the lift coefficient "Cl" is 1.088, this value is quite close to the value of the lift coefficient of 1.095, from equation (7), the deviation between the two values is 0.28% with respect to the Theodorsen method.

The aerodynamic profile, shown in Figure 1.6, is a medium thickness profile, the generation of the pressure coefficients is satisfactory, according to the Theodorsen method the lift coefficient "Cl" is 1.082, this value is quite close to the value of the lift coefficient of 1.095, from equation (7), the deviation between the two values is 1.2% with respect to the Theodorsen method.

The aerodynamic profile, shown in Figure 1.7, is a profile of medium thickness, the generation of the pressure coefficients is satisfactory, according to the Theodorsen method the lift coefficient "Cl" is 0.88, this value is close to the value of the lift coefficient of 1.095, from equation (7), however, the deviation has an important value between the two values, being 24.43% with respect to the Theodorsen method. The approximation has a substantial difference with respect to the method developed by Theodorsen, being in this case, the thickness of the profile the cause of the difference.

The aerodynamic profile, shown in Figure 1.8, is a profile of thin thickness, the generation of the pressure coefficients is satisfactory, according to the Theodorsen method the lift coefficient "Cl" is 0.68, this value deviates to the value of the lift coefficient of 1.095, from equation (7), however, the deviation between the two values is 61% with respect to the Theodorsen method. The approximation has a substantial difference with respect to the method developed by Theodorsen, being, in this case, the thickness of the profile the cause of the difference.

3. Analysis in Qblade

Qblade is a wind turbine calculation software, the integration of the XFOIL / XFLR5 functionality allows to design custom aerodynamic profiles and calculate their performance poles, this being an excellent tool for the purpose of research.

The results made it possible to obtain the angle of attack that provides the greatest aerodynamic finesse in addition to the drag and lift coefficients. Next, the figures of the graphs are presented, with parameters of the Reynolds number indicated in each of the figures of the order in millions of units.

ISSN 2523-6776

Figure 3.1, Figure 3.2 and Figure 3.3 are the results in the Qblade software of the R0.9B5 profile at different Reynolds numbers of the order of millions and different angles of attack.

Figure 3.1 shows that the highest coefficient of resistance occurs at an angle of attack of twenty degrees, this being around 0.09, however, they are satisfactory results due to their reduced magnitudes.

Figure 3.2 indicates that the lift coefficient falls at an angle of attack around 7.5, because the graphs of the lift coefficient against the angle of attack are no longer linear, the value at this angle of attack is 1.4.

Figure 3.3 shows that the best aerodynamic fineness produced by the profile occurs at an angle of attack of 4 degrees of camber, the corresponding value of the aerodynamic fineness at this angle of attack is around 140 to 155.

Figure 3.4, Figure 3.5 and Figure 3.6 and 3.6 are the results in the Qblade software of the profile R0.95B5 at different Reynolds numbers and angles of attack.

Figure 3.4 shows that the highest drag coefficient occurs at an angle of 20 degrees, the values of this coefficient increase dramatically after an angle of attack of 10 degrees. The magnitudes of the drag coefficients, for angles of attack less than 10 degrees, are less than 0.05, this result is quite satisfactory.

Figure 3.5 indicates that the lift coefficient does not drop to the angle of attack around ten degrees, this being a somewhat satisfactory result. The lift coefficient values range from 1.2 to 1.6.

Figure 3.6 shows that the best aerodynamic fineness produced by the profile is given at an angle of attack of 2.3 degrees of camber, the corresponding value of the aerodynamic fineness at this angle of attack is 130 to 157.

Figure 3.7, Figure 3.8 and Figure 3.9 are the results in the Qblade software of the profile R0.85B10.

Figure 3.7 shows that the highest drag coefficient occurs at an angle of attack around twenty degrees, this being its value between 0.09 and 0.1.

Figure 3.8 indicates that the lift coefficient does not drop at the angle of attack of about twenty degrees, this being a very satisfactory result. The lift coefficient values range from 1.8 to 2. Its graph is linear up to an angle of attack value of 7 degrees.

Figure 3.9 shows that the best aerodynamic fineness produced by the profile is given at an angle of attack of 4 degrees of lean, the corresponding value of the aerodynamic fineness at this angle of attack is 142 to 220.

Figures 3.10, 3.11 and 3.12 are the results in the Qblade software of the profile R0.87B10.

Figure 3.10 shows that the highest drag coefficient occurs at an angle of attack of around twenty degrees, this being its value between 0.8 and 0.12. However, under small angles of attack, the values of the drag coefficient are low.

Figure 3.11 indicates that the lift coefficient does not drop at the angle of attack of about eight degrees, this being a very satisfactory result. The lift coefficient values range from 1.7 to 1.8.

Figure 3.12 shows that the best aerodynamic fineness produced by the profile is given at an angle of attack of 4 degrees of lean, the corresponding value of the aerodynamic fineness at this angle of attack is 159 to 224.

Figure 3.13, Figure 3.14 and Figure 3.15 are the results in the Qblade software of the profile R0.9B10.

Figure 3.13 shows that the highest drag coefficient occurs at an angle of attack of around twenty degrees, this being its value between 0.8 and 0.12. However, the magnitudes of the drag coefficient are reduced for angles of attack less than 10 degrees.

ISSN 2523-6776

Figure 3.14 indicates that the lift coefficient does not drop to the angle of attack of about twenty degrees, this being a very satisfactory result. The lift coefficient values range from 1.5 to 1.9. It must be said that there is a variation in the graph within the line at an angle of attack of four degrees, however, this fact must be verified in a wind tunnel. The coefficient drops to an approximate angle of attack of 7 degrees.

Figure 3.15 shows that the best aerodynamic fineness produced by the profile is given at an angle of attack of 4 degrees lean, the corresponding value of the aerodynamic fineness at this angle of attack is between the range of 175 to 225.

Figure 3.16, Figure 3.17 and Figure 3.18 are the results in the Qblade software of the profile R0.92B10.

Figure 3.16 shows that the highest coefficient of resistance occurs at an angle of attack of around twenty degrees, this being its value between 0.07 and 0.16. For angles of attack less than 10 degrees, the magnitudes of the drag coefficient are less than 0.025, being a satisfactory result.

Figure 3.17 indicates that the lift coefficient does not drop to the angle of attack around eight degrees, this being a very satisfactory result. The lift coefficient values range from 1.6.

Figure 3.18 shows that the best aerodynamic fineness produced by the profile is given at an angle of attack between 4 to 5 degrees of lean, the corresponding value of the aerodynamic fineness at this angle of attack is 200 to 250.

The results in the XFOIL analysis are very close to that of equation number (7), this corroborates that the lift coefficients are close to those that the Kutta-Joukowsky theorem equation quantifies, the Theodorsen method instead is only Accurate for certain profiles of medium thickness and thick profiles.

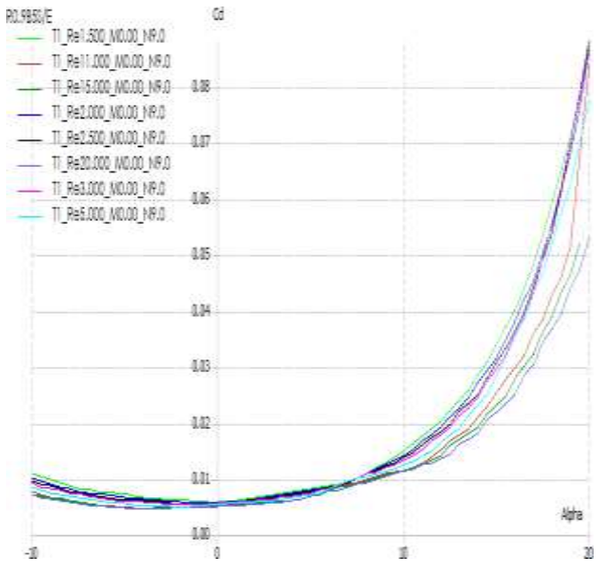

Figure 3.1 Results of the Qblade software of the profile R0.9B5 drag coefficient against the angle of attack.

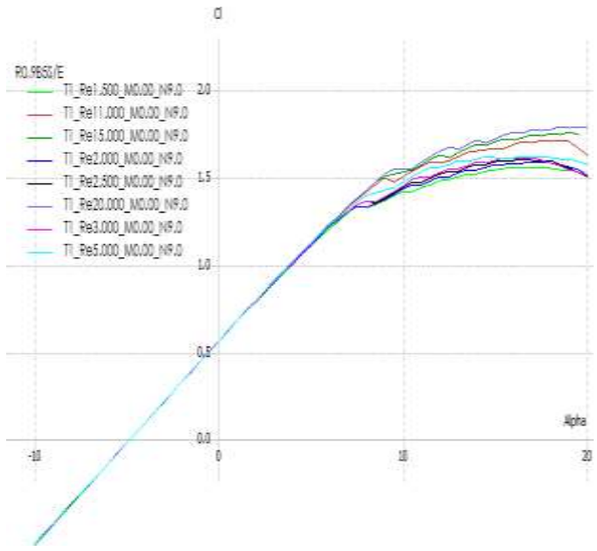

Figure 3.2 Results of the Qblade software of the R0.9B5 profile coefficient of lift versus angle of attack.

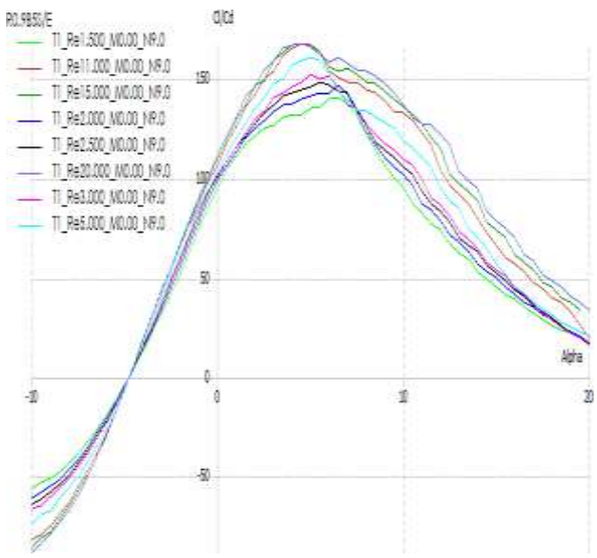

Figure 3.3 Results of the Qblade software of the profile R0.9B5 aerodynamic fineness against angle of attack.

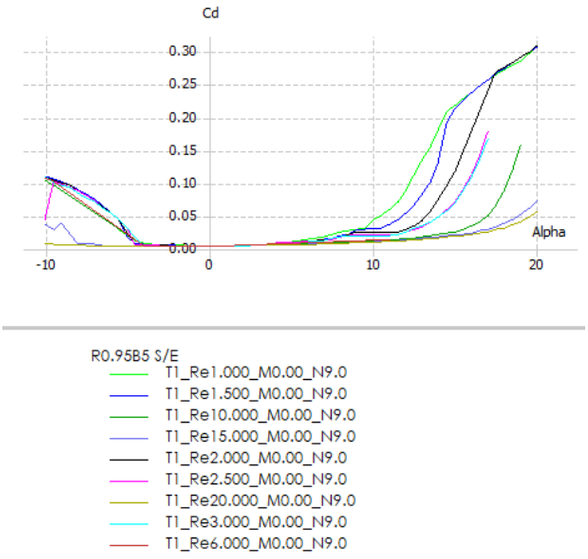

Figure 3.4 Qblade software results of the R0.9B5 profile coefficient of drag versus angle of attack.

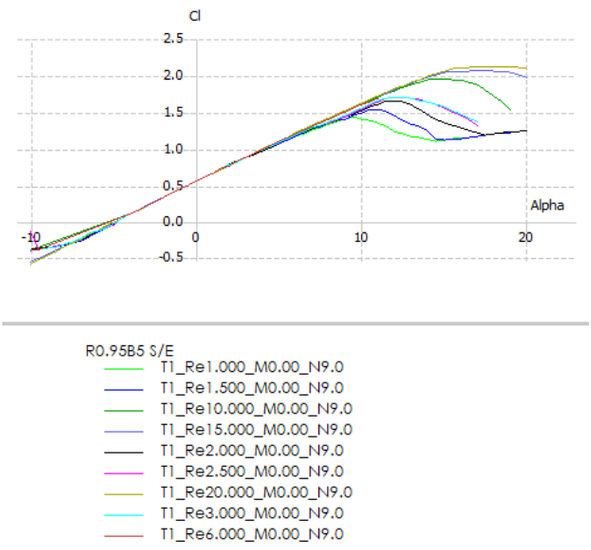

Figure 3.5 Results of the Qblade software of the R0.95B5 profile coefficient of lift versus angle of attack.

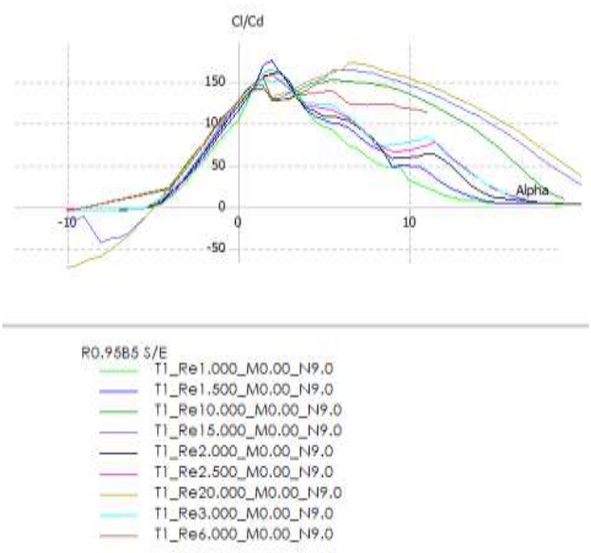

Figure 3.6 Results of the Qblade software of the profile R0.95B5 aerodynamic fineness against angle of attack.

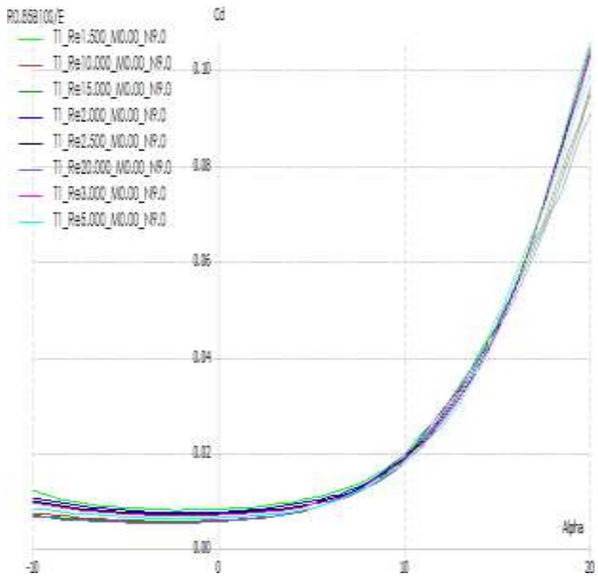

Figure 3.7 Qblade software results of profile R0.85B10 coefficient of drag versus angle of attack.

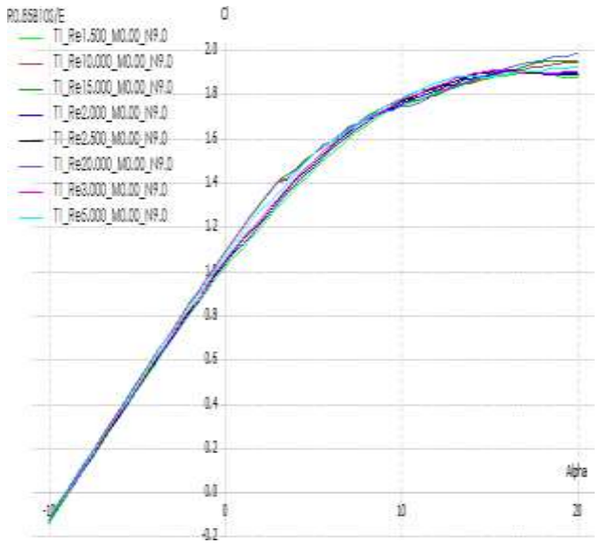

Figure 3.8 Qblade software results of the R0.85B10 profile coefficient of lift versus angle of attack.

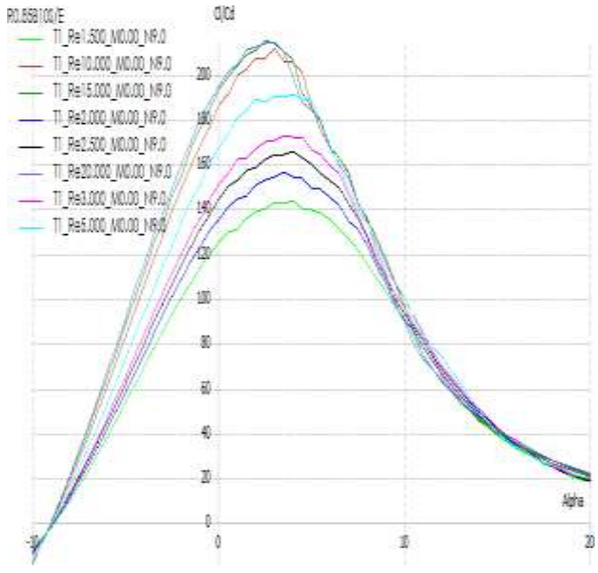

Figure 3.9 Results of the Qblade software of the profile R0.85B10 aerodynamic fineness against angle of attack.

ISSN 2523-6776

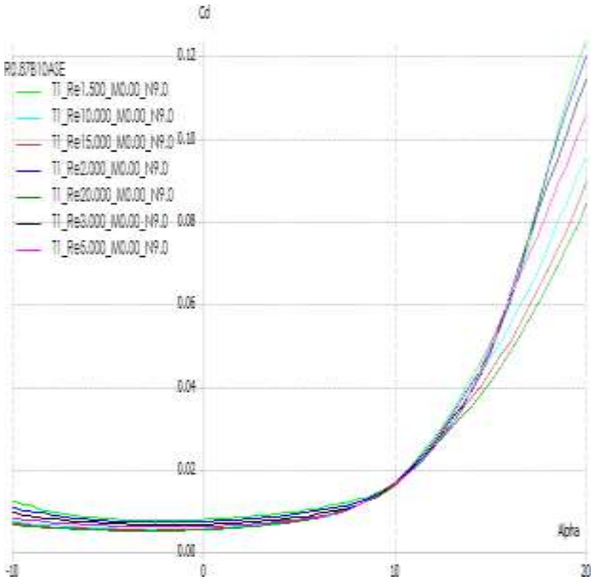

Figure 3.10 Results of the Qblade software of the profile R0.87B10 drag coefficient against the angle of attack.

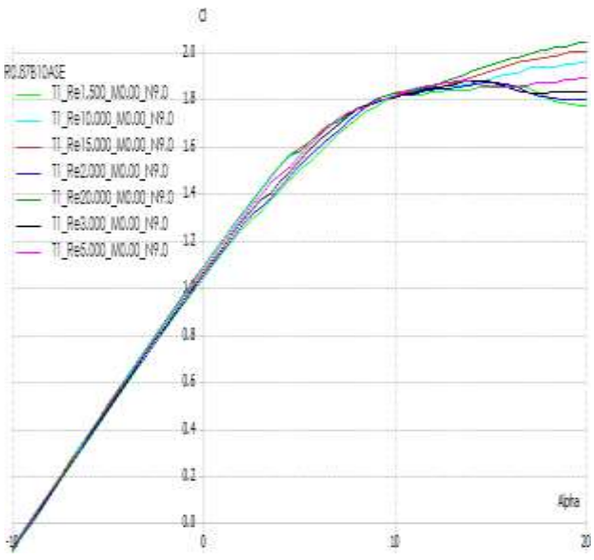

Figure 3.11 Results of the Qblade software of the profile R0.87B10 coefficient of lift against angle of attack

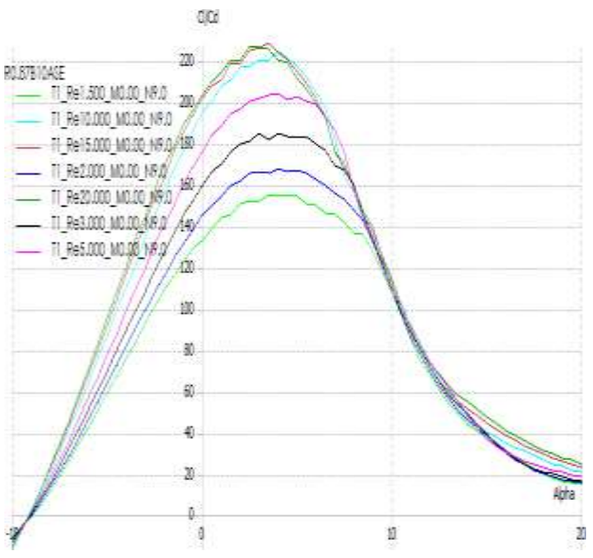

Figure 3.12 Results of the Qblade software of the profile R0.87B10 coefficient of lift against angle of attack

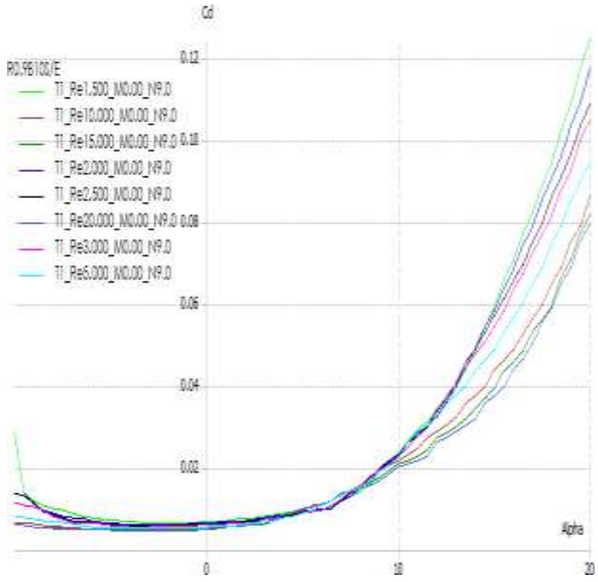

Figure 3.13 Results of the Qblade software of the profile R0.9B10 drag coefficient against the angle of attack.

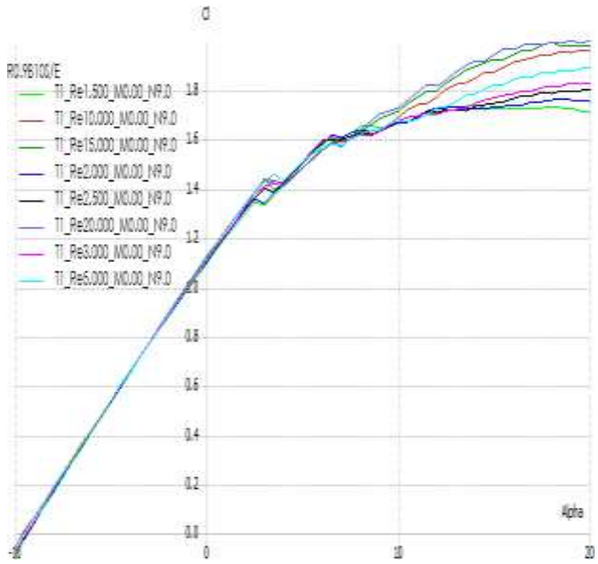

Figure 3.14 Results of the Qblade software of the profile R0.9B10 coefficient of lift versus angle of attack.

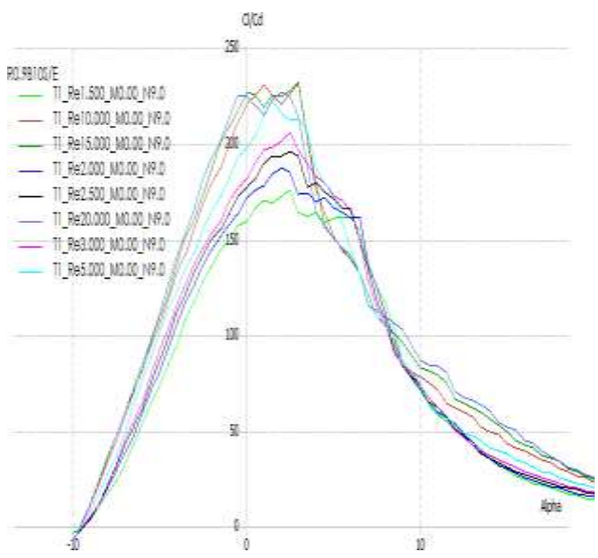

Figure 3.15 Results of the Qblade software of the profile R0.9B10 aerodynamic fineness against angle of attack.

ISSN 2523-6776

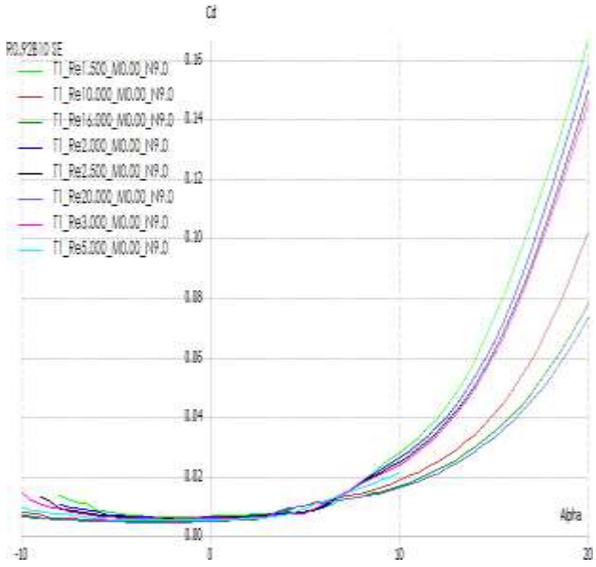

Figure 3.16 Qblade software results of profile R0.9B10 coefficient of drag versus angle of attack

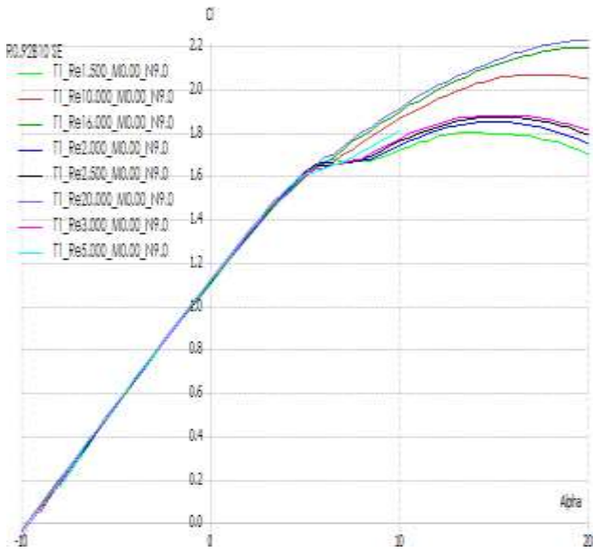

Figure 3.17 Results of the Qblade software of the profile R0.92B10 coefficient of lift against angle of attack

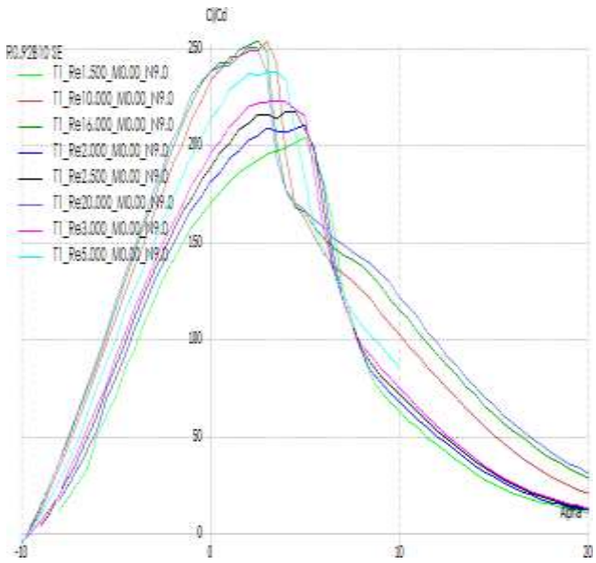

Figure 3.18 Results of the Qblade software of the profile R0.92B10 aerodynamic fineness against angle of attack.

4. Transition points of the wing profiles

The transition points are the coordinates defined in percentage of the chord where the laminar flow around the wing profile changes to a transitory or turbulent one due to the laminar separation bubble, these points are provided by the software, these coordinates being called "Upper trans "," Upper transition "refers to the transition in the upper surface, while the term" Lower trans "refers to" Lower transition ", which indicates the transition point of the flow in the intrados.

Profile R0.9B5A0		
Attack angle 0 °		
Reynolds	**Upper transition**	**Lower transition**
1.5x10^6	62.60%	30.30%
2x10^6	60.00%	27.50%
2.5x10^6	56.60%	25.80%
3x10^6	53.50%	24.10%
5x10^6	46.80%	20.70%
11x10^6	37.70%	16.30%
15x10^6	36.00%	14.20%
20x10^6	32.30%	14.00%

Table 4.1 Transition points of profile R0.9B5A0

Table 4.1 indicates that the profile achieves, for an angle of attack equal to zero, to generate under small Reynolds numbers, for example for a Reynolds number of 3 million, the laminar flow reaches up to 53.3% of its chord in the extrados , while in the intrados the laminar flow begins to form up to 24.1% of the chord of the wing profile, in addition, its performance for high Reynolds numbers, for example 11 million, is acceptable since the profile is capable to maintain a laminar flow up to 37.7% of its chord while the laminar flow in the ceiling appears up to 16.3% of it.

Table 4.2 indicates that the profile achieves, for an angle of attack equal to 2.5°, to generate under small Reynolds numbers, equal to 3 million, a laminar flow of up to 37.6% of its chord in the extrados, while in the intrados laminar flow begins to form up to 44.7% of the chord of the wing profile, in addition, its performance at high Reynolds numbers, of 11 million, allows a laminar flow to be obtained on most soffits but not on the extrados, since the profile is capable of maintaining laminar flow up to 28% of its chord while laminar flow in the intrados appears up to 29.5% of it.

ISSN 2523-6776

Table 4.3 indicates that the profile achieves, for an angle of attack equal to 5 °, to generate under small Reynolds numbers, than 3 million, a laminar flow up to 27.7% of its chord on the extrados, while in the intrados laminar flow begins to form up to 61% of the chord of the wing profile, in addition, its performance for high Reynolds numbers, than 11 million, allows a laminar flow to be obtained over most of the intrados but not over the extrados , since the profile is capable of maintaining laminar flow up to 17.1% of its chord while laminar flow in the intrados appears up to 48.6% of it.

Profile R0.9B5A2.5		
Angle of attack 2.5 °		
Reynolds	**Upper transition**	**Lower transition**
1.5x10^6	44.70%	53.80%
2x10^6	41.20%	50.20%
2.5x10^6	39.80%	47.30%
3x10^6	37.60%	44.70%
5x10^6	33.70%	38.90%
11x10^6	28.00%	29.50%
15x10^6	24.70%	26.30%
20x10^6	23.70%	24.10%

Table 4.2 Transition points of profile R0.9B5A2.5

Profile R0.9B5A5		
Angle of attack 5 °		
Reynolds	**Upper transition**	**Lower transition**
1.5x10^6	31.70%	67.70%
2x10^6	29.80%	65.10%
2.5x10^6	28.10%	63.30%
3x10^6	27.70%	61.00%
5x10^6	23.90%	58.00%
11x10^6	17.10%	48.60%
15x10^6	14.10%	44.60%
20x10^6	11.70%	40.60%

Table 4.3 Transition points of profile R0.9B5A5

Table 4.4 indicates that the profile achieves, for an angle of attack equal to 7.5 °, to generate under small Reynolds numbers, than 3 million, a laminar flow up to 11.4% of its chord on the extrados, while in the intrados the laminar flow is never formed, in addition, its performance for high Reynolds numbers, than 11 million, allows to obtain a laminar flow over most of the intrados but not over the extrados, since the profile is capable of maintaining a flow laminar up to 5% of its chord while laminar flow in the soffit appears up to 60.9% of it.

The tables of the transition points are located in the annexes, the first annex contains the tables of the transition points of the R0.95B5 profile, the second annex the tables of the R0.85B10 profile, the third annex the tables of the R0 profile. 87B10, the fourth appendix the tables of the profile R0.9B10 and the fifth the tables of the profile R0.92B10.

Profile R0.9B5A7.5		
ngle of attack 7.5 °		
Reynolds	**Upper transition**	**Lower transition**
1.5x10^6	20.30%	100.00%
2x10^6	16.50%	100.00%
2.5x10^6	13.50%	100.00%
3x10^6	11.40%	100.00%
5x10^6	7.80%	69.60%
11x10^6	5.00%	60.90%
15x10^6	3.60%	60.10%
20x10^6	2.50%	56.40%

Table 4.4 Transition points of profile R0.9B5A7.5

Conclusions

1. It was found that the curvature in the contour of the profile causes an increase in the lift coefficient, a fact that is corroborated by the circulation equation, and in addition, the relationship between the lift coefficient and the drag coefficient is wider, consequently A thin profile with the appropriate curvature generates a greater aerodynamic fineness compared to a thicker one, in addition, in theory the thin profile can develop a greater lift coefficient than a thick thick one, this can be observed if the performances performed by the profiles R0.92B10 and R0.87B10.

2. The Joukowsky transformation allows to obtain aerodynamic profiles with satisfactory performance values, but due to the uniqueness in the "-b" coordinate, the transformation generates a very sharp trailing edge.

3. Analysis by Theodorsen method is not effective for thin and some medium airfoils, check Table 1 from the annex 6.

4. Thicker profiles tend to perform better at high angles of attack compared to thinner profiles.

ISSN 2523-6776

5. The thicker profiles better preserve the boundary layer on the surface by increasing the angle of attack compared to the thin profiles, see tables of the transition points of profile R0.85B10.

6. Thin wing profiles at high angles of attack generate very high drag coefficients and turbulent flows over the surface, see profile tables R0.95B5, R0.9B5, R0.92B10 and R0.9B10.

7. It was found that, in theory, as the Reynolds number increases, the flow on the upper surface becomes turbulent, while on the lower surface the flow becomes laminar.

Acknowledgements

To the Universidad Michoacana de San Nicolás de Hidalgo for providing the tools for research.

To FIM, Facultad de Ingeniería Mecánica
.
To the RETANA-VEGA, Dzoara, Estefanía. BsC, for her support in this work.

Annexes

Annex 1

Table 4.5 indicates that the R0.95B5 profile achieves, for an angle of attack equal to zero, to generate under small Reynolds numbers, than 3 million, a laminar flow up to 69% of its chord on the extrados, while in the intrados the laminar flow begins to form up to 27.4% of the chord of the wing profile, in addition, its performance for high Reynolds numbers, than 11 million, is satisfactory since the profile is capable of maintaining a laminar flow up to 49.1% of its chord while laminar flow in the soffit appears up to 13.9% of it.

Profile R0.95B5A0		
Attack angle 0 °		
Reynolds	**Upper transition**	**Lower transition**
1.5x10^6	75.80%	34.10%
2x10^6	73.50%	31.10%
2.5x10^6	71.20%	29.10%
3x10^6	69.00%	27.40%
5x10^6	60.40%	20.70%
11x10^6	49.10%	13.90%
15x10^6	44.00%	12.00%
20x10^6	38.80%	10.30%

Table 4.5 Transition points of profile R0.95B5A0

Table 4.6 indicates that the profile achieves, for an angle of attack equal to 3 °, to generate under small Reynolds numbers, of 3 million, a laminar flow of up to 19.8% of its chord on the extrados, although it is important Note that at this angle of attack, the boundary layer is dramatically affected in a negative way as the Reynolds number increases in the analyzes, in the intrados no laminar flow is generated at any point of the chord of the wing profile, in addition , its performance for high Reynolds numbers, higher than 11 million, allows a laminar flow to be obtained over most of the intrados but not over the extrados, since the profile is capable of maintaining a laminar flow up to 3.7% of its chord while laminar flow in the soffit appears up to 41.2% of it.

Profile R0.95B5A3		
Angle of attack 3 °		
Reynolds	**Upper transition**	**Lower transition**
1.5x10^6	40.90%	100.00%
2x10^6	31.60%	100.00%
2.5x10^6	24.40%	100.00%
3x10^6	19.80%	100.00%
5x10^6	10.80%	69.60%
11x10^6	3.70%	41.20%
15x10^6	3.20%	34.40%
20x10^6	1.50%	27.70%

Table 4.6 Transition points of profile R0.95B5A3

Profile R0.95B5A7		
Angle of attack 7 °		
Reynolds	**Upper transition**	**Lower transition**
1.5x10^6	0.50%	100.00%
2x10^6	0.40%	100.00%
2.5x10^6	0.30%	100.00%
3x10^6	0.30%	100.00%
5x10^6	0.30%	100.00%
11x10^6	0.20%	100.00%
15x10^6	0.20%	100.00%
20x10^6	0.20%	100.00%

Table 4.7 Transition points of profile R0.95B5A7

Table 4.7 indicates that the profile R0.95B5A7 achieves, for an angle of attack equal to 7 °, to generate under small Reynolds numbers, than 3 million, a laminar flow up to 0.3% of its chord on the extrados, while in the intrados does not generate laminar flow, in addition, its performance for high Reynolds numbers, greater than 11 million, the profile maintains its laminar flow up to 0.2% of its chord on the extrados, on the other hand, in the intrados, all the flow on the surface it is turbulent.

Annex 2

Table 4.8 indicates that the R0.85B10 profile achieves, for an angle of attack equal to zero, to generate under small Reynolds numbers, than 3 million, a laminar flow of 53.9% of its chord on the extrados, while in the intrados the laminar flow begins to form up to 17.8% of the chord of the wing profile, in addition, its performance for high Reynolds numbers, than 10 million, is acceptable since the profile is capable of maintaining a laminar flow up to the 48.2% of its chord while laminar flow in the soffit appears up to 14.3% of it.

Profile R0.85B10A0		
Attack angle 0 °		
Reynolds	**Upper transition**	**Lower transition**
1.5x10^6	56.80%	19.80%
2x10^6	55.50%	18.90%
2.5x10^6	54.60%	18.40%
3x10^6	53.90%	17.80%
5x10^6	51.40%	16.50%
10x10^6	48.20%	14.30%
15x10^6	45.70%	13.00%
20x10^6	43.40%	12.30%

Table 4.8 Transition points of profile R0.85B10A0

Profile R0.85B10A3		
Angle of attack 3 °		
Reynolds	**Upper transition**	**Lower transition**
1.5x10^6	51.90%	27.80%
2x10^6	50.60%	26.50%
2.5x10^6	49.60%	26.10%
3x10^6	48.50%	25.70%
5x10^6	46.10%	23.70%
10x10^6	41.70%	22.30%
15x10^6	37.70%	21.10%
20x10^6	35.20%	19.80%

Table 4.9 Transition points of profile R0.85B10A3

Table 4.9 indicates that the profile achieves, for an angle of attack equal to 3 °, to generate under small Reynolds numbers, than 3 million, a laminar flow of 48.5% of its chord on the extrados, while on the intrados laminar flow begins to form up to 25.7% of the chord of the wing profile, in addition, its performance for high Reynolds numbers, than 10 million, is acceptable since the profile is capable of maintaining a laminar flow up to 41.7% of its chord while laminar flow in the soffit appears up to 22.3% of it.

Table 4.10 indicates that the profile achieves, for an angle of attack equal to 7 °, to generate under small Reynolds numbers, than 3 million, a laminar flow of 39.2% of its chord on the extrados, while in the intrados laminar flow begins to form up to 37.7% of the chord of the wing profile, in addition, its performance for high Reynolds numbers, than 10 million, is acceptable since the profile is capable of maintaining a laminar flow up to 26.4% of its chord while the laminar flow in the intrados appears up to 31.4% of it.

Profile R0.85B10A7		
Angle of attack 7 °		
Reynolds	**Upper transition**	**Lower transition**
1.5x10^6	44.00%	42.60%
2x10^6	42.10%	40.50%
2.5x10^6	40.70%	39.20%
3x10^6	39.20%	37.70%
5x10^6	33.00%	34.60%
10x10^6	26.40%	31.40%
15x10^6	22.20%	28.90%
20x10^6	19.30%	28.20%

Table 4.10 Transition points of profile R0.85B10A7

Table 4.11 indicates that the profile achieves, for an angle of attack equal to 14 °, to generate under small Reynolds numbers, than 3 million, a laminar flow up to 17.7% of its chord on the extrados, while in the intrados the flow is never laminar, in addition, for high Reynolds numbers, than 10 million, the profile is capable of maintaining a laminar flow up to 5.3% of its chord while the laminar flow in intrados is never generated.

Profile R0.85B10A14		
Angle of attack 14 °		
Reynolds	**Upper transition**	**Lower transition**
1.5x10^6	22.30%	100.00%
2x10^6	20.50%	100.00%
2.5x10^6	19.00%	100.00%
3x10^6	17.70%	100.00%
5x10^6	12.50%	100.00%
10x10^6	5.30%	100.00%
15x10^6	2.90%	60.30%
20x10^6	1.70%	53.90%

Table 4.11 Transition points of profile R0.85B10A14

ISSN 2523-6776

Table 4.12 indicates that the profile achieves, for an angle of attack equal to 20 °, to generate under small Reynolds numbers, than 3 million, a laminar flow up to 5.4% of its chord on the extrados, while in the intrados the flow is never laminar, in addition, for high Reynolds numbers, than 10 million, the profile is capable of maintaining a laminar flow up to 1.3% of its chord while the laminar flow in intrados is never generated again.

Profile R0.85B10A20		
Angle of attack 20°		
Reynolds	**Upper transition**	**Lower transition**
1.5x10^6	9.00%	100.00%
2x10^6	7.40%	100.00%
2.5x10^6	6.10%	100.00%
3x10^6	5.40%	100.00%
5x10^6	3.50%	100.00%
10x10^6	1.30%	100.00%
15x10^6	0.50%	100.00%
20x10^6	0.40%	100.00%

Table 4.12 Transition points of profile R0.85B10A20

Annex 3

Profile R0.87B10A0		
Attack angle 0°		
Reynolds	**Upper transition**	**Lower transition**
1.5x10^6	57.20%	19.80%
2x10^6	56.30%	19.10%
2.5x10^6	55.10%	18.50%
3x10^6	54.40%	17.80%
5x10^6	52.00%	16.10%
10x10^6	48.90%	13.90%
15x10^6	46.20%	13.00%
20x10^6	43.70%	12.00%

Table 4.13 Transition points of profile R0.87B10A0

Table 4.13 indicates that the profile achieves, for an angle of attack equal to zero, to generate under small Reynolds numbers, than 3 million, a laminar flow up to 54.4% of its chord on the extrados, while on the intrados laminar flow begins to form up to 17.8% of the chord of the wing profile, in addition, its performance for high Reynolds numbers, than 10 million, is satisfactory since the profile is capable of maintaining a laminar flow up to 48.9% of its chord while the laminar flow in the soffit appears up to 13% of it.

Table 4.14 indicates that the profile achieves, for an angle of attack equal to 3 °, to generate under small Reynolds numbers, than 3 million, a laminar flow up to 48.7% of its chord on the extrados, while in the intrados the laminar flow begins to form up to 25.3% of the chord of the wing profile, in addition, its performance for high Reynolds numbers, than 10 million, allows to obtain a laminar flow, since the profile is capable of maintaining a flow laminar up to 41.5% of its chord while laminar flow in the soffit appears up to 21.7% of it.

Profile R0.87B10A3		
Angle of attack 3 °		
Reynolds	**Upper transition**	**Lower transition**
1.5x10^6	52.00%	27.20%
2x10^6	50.90%	25.90%
2.5x10^6	49.60%	25.60%
3x10^6	48.70%	25.30%
5x10^6	45.90%	23.60%
10x10^6	41.50%	21.70%
15x10^6	38.60%	21.10%
20x10^6	35.80%	19.90%

Table 4.14 Transition points of profile R0.87B10A3

Table 4.14 indicates that the profile achieves, for an angle of attack equal to 3 °, to generate under small Reynolds numbers, than 3 million, a laminar flow up to 48.7% of its chord on the extrados, while in the intrados the laminar flow begins to form up to 25.3% of the chord of the wing profile, in addition, its performance for high Reynolds numbers, than 10 million, allows to obtain a laminar flow, since the profile is capable of maintaining a flow laminar up to 41.5% of its chord while laminar flow in the soffit appears up to 21.7% of it.

Profile R0.87B10A5		
Angle of attack 5 °		
Reynolds	**Upper transition**	**Lower transition**
1.5x10^6	48.30%	33.60%
2x10^6	46.80%	32.50%
2.5x10^6	45.60%	31.20%
3x10^6	44.60%	30.70%
5x10^6	42.00%	28.40%
10x10^6	36.90%	25.90%
15x10^6	30.30%	25.80%
20x10^6	28.80%	23.60%

Table 4.15 Transition points of profile R0.87B10A5

ISSN 2523-6776

Table 4.15 indicates that the profile achieves, for an angle of attack equal to 5 °, to generate under small Reynolds numbers, than 3 million, a laminar flow up to 44.6% of its chord on the extrados, while in the intrados the laminar flow begins to form up to 30.7% of the chord of the wing profile, in addition, its performance for high Reynolds numbers, than 10 million, allows to obtain a laminar flow, since the profile is capable of maintaining a flow laminar up to 36.90% of its chord while laminar flow in the soffit appears up to 25.8% of it.

Profile R0.87B10A7.5		
Angle of attack 7.5 °		
Reynolds	**Upper transition**	**Lower transition**
1.5x10^6	43.50%	54.70%
2x10^6	41.80%	49.40%
2.5x10^6	40.10%	46.10%
3x10^6	39.30%	44.40%
5x10^6	34.60%	39.20%
10x10^6	24.40%	33.40%
15x10^6	19.00%	32.70%
20x10^6	18.60%	29.20%

Table 4.16 Transition points of profile R0.87B10A7.5

Table 4.16 indicates that the profile achieves, for an angle of attack equal to 7.5 °, to generate under small Reynolds numbers, than 3 million, a laminar flow up to 39.3% of its chord on the extrados, while in the intrados the laminar flow begins to form up to 44.4% of the chord of the wing profile, in addition, its performance for high Reynolds numbers, than 10 million, allows to obtain a laminar flow up to 24.4% of its chord while the flow laminar on the intrados appears up to 33.4% of it.

Profile R0.87B10A10		
Angle of attack 10 °		
Reynolds	**Upper transition**	**Lower transition**
1.5x10^6	34.80%	100.00%
2x10^6	31.20%	100.00%
2.5x10^6	28.20%	100.00%
3x10^6	25.70%	100.00%
5x10^6	20.00%	68.30%
10x10^6	14.70%	46.00%
15x10^6	11.20%	40.80%
20x10^6	8.20%	37.70%

Table 4.17 Transition points of profile R0.87B10A10

Table 4.17 indicates that the profile achieves, for an angle of attack equal to 10 °, to generate under small Reynolds numbers, less than 3 million, a laminar flow up to 25.7% of its chord on the extrados, while in the intrados laminar flow does not appear for these conditions, its performance for high Reynolds numbers, greater than 10 million, the profile is capable of maintaining laminar flow up to 14.7% of its chord while laminar flow in the intrados appears up to 46% of it.

Annex 4

Profile R0.9B10A0		
Attack angle 0 °		
Reynolds	**Upper transition**	**Lower transition**
1.5x10^6	61.50%	18.50%
2x10^6	60.40%	16.60%
2.5x10^6	59.00%	16.10%
3x10^6	57.20%	15.30%
5x10^6	55.10%	13.40%
10x10^6	52.00%	10.70%
15x10^6	48.90%	9.20%
20x10^6	44.90%	8.60%

Table 4.18 Transition points of profile R0.9B10A0

Table 4.18 indicates that the profile achieves, for an angle of attack equal to zero, to generate under small Reynolds numbers, than 3 million, a laminar flow up to 57.7% of its chord on the extrados, while in the intrados laminar flow begins to form up to 15.3% of the chord of the wing profile, in addition, its performance for high Reynolds numbers, than 10 million, is very satisfactory since the profile is capable of maintaining a laminar flow up to 52 % of its chord while laminar flow in the intrados appears up to 10.7% of it.

Profile R0.9B10A3		
Angle of attack 3 °		
Reynolds	**Upper transition**	**Lower transition**
1.5x10^6	54.90%	31.80%
2x10^6	53.00%	30.90%
2.5x10^6	51.40%	30.90%
3x10^6	48.90%	29.80%
5x10^6	44.80%	28.10%
10x10^6	40.50%	25.20%
15x10^6	36.50%	22.40%
20x10^6	32.70%	19.40%

Table 4.19 Transition points of profile R0.9B10A3

ISSN 2523-6776

Table 4.19 indicates that the profile achieves, for an angle of attack equal to 3 °, to generate under small Reynolds numbers, than 3 million, a laminar flow up to 48.9% of its chord on the extrados, while in the intrados the laminar flow begins to form up to 29.8% of the chord of the wing profile, in addition, its performance for high Reynolds numbers, than 10 million, is satisfactory since the profile is capable of maintaining a laminar flow up to 40.5 % of its chord while laminar flow in the intrados appears up to 25.2% of it.

Profile R0.9B10A6		
Attack angle 6 °		
Reynolds	**Upper transition**	**Lower transition**
1.5x10^6	44.70%	100.00%
2x10^6	41.20%	67.60%
2.5x10^6	39.70%	56.80%
3x10^6	36.70%	47.50%
5x10^6	24.00%	37.70%
10x10^6	13.40%	32.00%
15x10^6	8.50%	30.80%
20x10^6	4.60%	29.00%

Table 4.20 Transition points of profile R0.9B10A6

Table 4.20 indicates that the profile achieves, for an angle of attack equal to 6 °, to generate under small Reynolds numbers, than 3 million, a laminar flow up to 36.7% of its chord on the extrados, while in the intrados the laminar flow begins to form up to 47.5% of the chord of the wing profile, in addition, its performance for high Reynolds numbers, than 10 million, the profile is capable of maintaining a laminar flow up to 13.4% of its chord while laminar flow in the intrados appears up to 32% of it.

Profile R0.9B10A8		
Angle of attack 8 °		
Reynolds	**Upper transition**	**Lower transition**
1.5x10^6	33.50%	100.00%
2x10^6	26.60%	100.00%
2.5x10^6	21.20%	100.00%
3x10^6	17.70%	100.00%
5x10^6	11.30%	100.00%
10x10^6	4.60%	42.70%
15x10^6	1.60%	37.70%
20x10^6	0.70%	35.10%

Table 4.21 Transition points of profile R0.9B10A8

Table 4.21 indicates that the profile achieves, for an angle of attack equal to 8 °, to generate under small Reynolds numbers, than 3 million, a laminar flow up to 17.7% of its chord on the extrados, while in the intrados the flow is never generated, in addition, its performance for high Reynolds numbers, than 10 million, the profile is capable of maintaining a laminar flow up to 4.6% of its chord while the laminar flow in the intrados appears up to 42.7 % Of the same.

Annex 5

Table 4.22 indicates that the profile achieves, for an angle of attack equal to zero, to generate under small Reynolds numbers, than 3 million, a laminar flow up to 61.8% of its chord on the extrados, while on the intrados laminar flow begins to form up to 14% of the chord of the wing profile, in addition, its performance for high Reynolds numbers, greater 10 million, is satisfactory since the profile is capable of maintaining a laminar flow up to 55% of its chord while laminar flow in the soffit appears up to 10% of it.

Profile R0.92B10A0		
Attack angle 0 °		
Reynolds	**Upper transition**	**Lower transition**
1.5x10^6	65.80%	16.60%
2x10^6	64.10%	15.30%
2.5x10^6	62.50%	14.70%
3x10^6	61.80%	14.00%
5x10^6	59.10%	12.40%
10x10^6	55.00%	10.00%
16x10^6	51.10%	9.10%
20x10^6	48.40%	8.30%

Table 4.22 Transition points of profile R0.92B10A0

Profile R0.92B10A3		
Angle of attack 3 °		
Reynolds	**Upper transition**	**Lower transition**
1.5x10^6	58.60%	39.50%
2x10^6	57.00%	36.70%
2.5x10^6	55.20%	34.80%
3x10^6	53.80%	33.20%
5x10^6	50.00%	29.80%
10x10^6	45.00%	24.90%
16x10^6	38.50%	21.80%
20x10^6	33.60%	21.00%

Table 4.23 Transition points of profile R0.92B10A3

ISSN 2523-6776

Table 4.23 indicates that the profile achieves, for an angle of attack equal to 3 °, to generate under small Reynolds numbers, than 3 million, a laminar flow up to 53.8% of its chord on the extrados, while in the intrados the laminar flow begins to form up to 33.2% of the chord of the wing profile, in addition, its performance for high Reynolds numbers, than 10 million, is satisfactory since the profile is capable of maintaining a laminar flow up to 45 % of its chord while laminar flow in the intrados appears up to 24.9% of it.

Table 4.24 indicates that the profile achieves, for an angle of attack equal to 5 °, to generate under small Reynolds numbers, than 3 million, a laminar flow up to 42.6% of its chord on the extrados, while in the intrados the laminar flow begins to form up to 93% of the chord of the wing profile, in addition, its performance for high Reynolds numbers, than 10 million, the profile is capable of maintaining a laminar flow up to 12.7% of its chord while the laminar flow in the intrados appears up to 35.5% of it.

Profile R0.92B10A5		
Angle of attack 5 °		
Reynolds	**Upper transition**	**Lower transition**
1.5x10^6	51.80%	100.00%
2x10^6	48.00%	100.00%
2.5x10^6	45.2%	100.00%
3x10^6	42.60%	93.00%
5x10^6	29.80%	45.80%
10x10^6	12.70%	35.50%
16x10^6	7.50%	31.40%
20x10^6	5.40%	30.20%

Table 4.24 Transition points of profile R0.92B10A5

Annex 6

Comparison of the results of the lift coefficients, at an angle identical to zero					
0	**1**	**2**	**3**	**4**	**5**
Profile name	Cl of the equation (3.6.6.1)	Cl of the analysis in the XFLR5 softwar, in Qblade	Cl of Theodorsen's method	Percentage difference of 1 with respect to 2	Percentage difference of 3 with respect to 2
R0.9B5A0	0.54	0.56	0.73	3.57%	-30.35%
R0.95B5A0	0.54	0.54	0.4	0%	25.9%
R0.85B10A	1.09	1.05	1.088	-3.8%	-3.61%
R0.87B10A0	1.09	1.06	1.082	-2.83	-2.075%
R0.9B10A0	1.09	1.1	0.88	0.9%	20%
R0.92B10A0	1.09	1.11	0.68	1.8%	38.73%

Table 1 Comparison of the results between the three methodologies

References

Carmona, Anibal Isidoro. *Aerodinámica y actuaciones del avion.* Madrid : Paraninfo, 2000.

Chattot, J.J y Hafez, M.M. *Theoretical and Applied Aerodynamics.* New York : Springer, 2015.

Galindo, Diego Rodrigo Flores. *Diseño de perfiles aerodinámicos.* Ciudad de México : s.n., 2006.

Gómez, Gabriel Adrián Romero. *Diseño de perfiles alares.* Morelia : s.n., 2021.

H. Abbott, Ira y Von Doenhoff, Albert E. *Theory of wing section.* New York : McGraw-Hill, 1959.

John D. Anderson, Jr. *Fundamentals of Aerodynamics.* Maryland : McGraw-Hill, 1991.

Katz, Joseph y Plotkin, Allen. *Low-Speed Aerodynamics.* New York : Cambrige University press, 2010.

McCormick, Barnes W. *Aerodinamics, aeronautics, and flight mechanics.* New York : Pennsylvania State University, 1979.

Tejada, Lina Alejandra. *Estudio de algunos perfiles aerodinámicos.* Bogotá : s.n., 2020.

White, Frank M. *Mecánica de fluidos.* s.l. : McGraw-Hill, 2010.

Article **Journal of Technological Engineering**
June, 2021 Vol.5 No.15 36-45

Mathematical modeling of a MOSFET transistor as modulator in AM transmission

Modelado Matemático de un transistor MOSFET como modulador en transmisión en AM

MOTA-GALVÁN, Eduardo†*& REYES-MARTINEZ, Roberto Alejandro

Universidad Autónoma de Baja California, Faculty of Chemical Sciences and Engineering

ID 1st Author: *Eduardo, Mota-Galván* / **ORC ID**: 0000-0003-3380-6759

ID 1st Co-author: *Roberto Alejandro, Reyes-Martinez* / **ORC ID**: 0000-0003-2210-2692, **Researcher ID Thomson**: AAN-2895-2020, **CVU CONACYT ID**: 21470

DOI: 10.35429/JTEN.2021.15.5.36.45 Received March 14, 2021; Accepted June 29, 2021

Abstract

The necessary methodology is presented to characterize the alternating signal transistor in the time and frequency domain and obtain its characteristic equations including its transfer function. The behavior of the transistor gate is studied in different models of manufacturers in alternating signal, therefore the difference between the behavior relationship between the theory and the information obtained in the experimentation is shown. All of the above to have an optimization, control or description of the operation of a real transistor and be used in an electrical / electronic application in general, in this case, for an AM modulation.

MOSFET, Mathematical modeling, Modulated amplitude

Resumen

Se presenta la metodología necesaria para caracterizar el transistor en señal alterna en el dominio temporal y frecuencial y obtener su(s) ecuaciones características incluyendo la función de transferencia del mismo. Se estudia el comportamiento de la compuerta del transistor en diferentes modelos de fabricantes en señal alterna por tanto se muestra la diferencia entre la relación de comportamiento entre lo teoría y la información obtenida en la experimentación. Todo lo anterior para tener una optimización, control o descripción del funcionamiento de un transistor real y ser aprovechado en una aplicación eléctrica/electrónica en general, para este caso, para una modulación AM.

MOSFET, Modelado matemático, Amplitud modulada

Citation: MOTA-GALVÁN, Eduardo & REYES-MARTINEZ, Roberto Alejandro. Mathematical modeling of a MOSFET transistor as modulator in AM transmission. Journal of Technological Engineering. 2021. 5-15: 36-45

* Correspondence to Author (e-mail: eduardo.mota@uabc.edu.mx)
† Researcher contributing as first author.

1 Introduction

The amplitude modulation is the process to modify the amplitude of a carrier signal, usually high frequency sinusoidal, commonly in RF spectrum, proportionally to the value of amplitude of a low frequency modulator signal [1]. Compared to other forms of modulation, AM modulation is easier, with the disadvantage of low quality signal. To modulate in AM it is necessary to use no lineal devices or signal multipliers.

There are two types of AM:

– DSBFC (double side band full carrier) is the easier method and common to make it. It is called double side band because, in the frequency domain, the bandwidth of the modulating signal is on both sides of carrier signal. Therefore the bandwidth of transmission is two times the frequency of modulating signal causing a loss in the bandwidth in the spectrum.

– SSB (single side band) in this type of modulation, it is only transmitted one of both side band of information, eliminating the carrier signal and the excess side band. The disadvantages are the bad quality sound compared with DSBFC AM, as well as the signal reception is more complex.

A lot of source of information either bibliography or digital, they explain the theoretical form of Am using established mathematical equations depending of the transmitter circuit. This transmitter usually is built with BJT transistor or JFET transistor. This transistors usually appear in the bibliography with a schematic diagram with some equation explaining the behavior of the transmitter.

However, the information is limited about the AM using MOSFET transistors at least in the traditional form of amplitude modulation without explaining of the behavior, matheatical equation or any transference function that allows to know the model.

From this some questions arise for modulators with BJTs or JFETs:

Where does the equation for the behavior of the transistor come from? What physical-mathematical criteria did they use to obtain it? Why don't they usually use AM modulators with MOSFETs if it is a power device with better efficiency, compared for example with a BJT?

It is important to know the origins and criteria to develop the equation of transmitter and this form take advantage the experience and knowledge to modeling other transistors or devices. If it is possible also apply the above in bibliography or exercises in laboratory practices. The central hypothesis of this investigation is the possibility to make an amplitude modulation taking advantage the no lineal behavior of MOSFET Gate transistor consider the transistor is stable to high frequency.

With the data from measurements it is possible to find behavior equations in time and frequency domain and lay the groundwork to the characterization of any transistor or device.

In this article talks about of the form of characterize a channel N MOSFET transistor, for that is presented the section of methodology, test prototype implementation, results obtained, conclusions and future work.

2 Metodología

The process of obtain data as well as the develop of characterization/modeling is recommended take in consideration the flow diagram which is presented in fig. 1

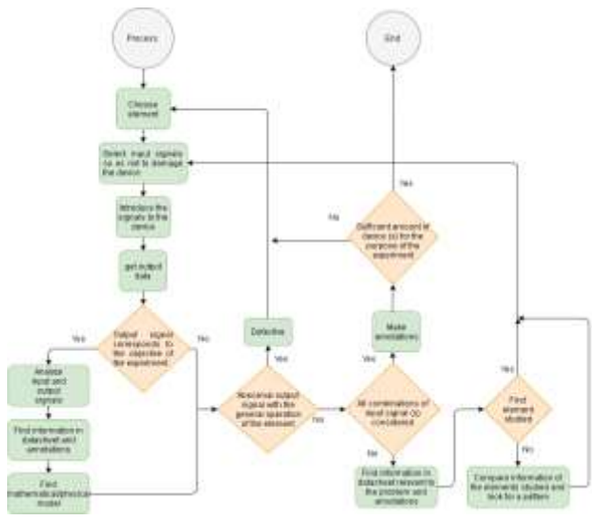

Figure 1 Process to obtain data
Source: Own Elaboration

ISSN 2523-6776

In the figure 1, it shows the methodology to make test measurements of any element or device, to know if the element is defective or if the quantity of test elements are enough to the investigation. To find the appropriate mathematical or physical model, the methodology used is presented in the figure 2.

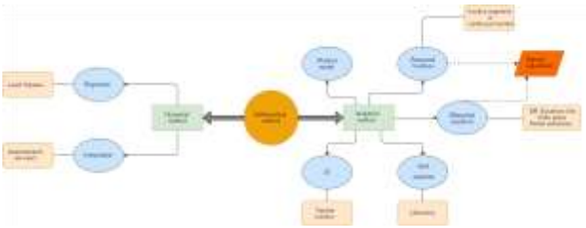

Figura 2 Process to select a mathematical model
Source: Own Elaboration

2.1 Modeling (data fit)

When an experiment is developing, it is necessary capture input and output values to understand the behavior of the experiment or the element to obtain an appropriate model acceptable; considering the method is not exact due approximations in the experiment or errors in the measurements for example inherent, truncation or rounding. For this is considered to use common methods for example regression or approximation method, interpolation method and analytic method which will give a brief explanation.

2.2 Regression or approximation method

By definition this method is a relationship that allows predict the probably values of one variable from another variable. This method is used when is desired a function that approximate the data obtained due errors in measurements or in devices. The order of the function is minor than quantity of points obtained in the measurements. There are distinct types of regression: lineal, quadratic, logaritmic, exponential, polynomial and least squares [2][3].

2.3 Interpolation Method

By definition the interpolation method is the estimation of a value of the variable y for a certain value of the variable x. This method is used when is desired a function to connect each of the data obtained, assuming that the measurements or the devices are exact and there is no error. The maximum power of an interpolation polynomial function is equal to the number of points minus one [4].

2.4 Analytic method

This method is the most “exact” because only use mathematical functions such as polynomials, algebraic or trigonometric functions that approximate the data, without use directly the data obtained from the experiment, it means, it is used only as a comparison graph of the results with the proposed model. The selection of an analytical method depends on the characteristics of the element or experiment [5].

Once identified the possible methods to proceed to modeling, it is necessary to identify an element of study, which for the interest of this investigation turns out to be the MOSFET transistor that is briefly described.

MOSFET transistor

The MOSFET transistor is a transistor whose operation is different from a BJT transistor. In a BJT transistor, the current that flows through it is controlled by an input current, it means, it is a current device controlled by current. However the MOSFET transistor is a transistor where the current flow from pin D to pin S being controlled by voltage across pin G.

Where the 'D' connector represents the drain which is where the current enters and the 'S' connector is the source where the current leaves. The main structure of a MOSFET transistor is a metal oxide semiconductor capacitor that corresponds to the gate (G), this capacitor is isolated from the semiconductor substrate that represents the drain and the source.

The semiconductor substrate can be made of material N or material P, depending on the type of material the voltage V can be negative or positive. For example, in the case of a P-type substrate, it is necessary for the voltage to be positive at the G pin so that the few free electrons found in the substrate are attracted by the electric field generated. In this form, the electrons will produce an "enrichment" segment in the substrate, creating an N-type channel through which the input current to the transistor can pass. If the substrate is made of N material, a P-type channel will be created. The enrichment channel is volumetric, that is, it has a length and width defined by the manufacturer [6].

ISSN 2523-6776

Starting with the use of an N-channel MOSFET transistor, will be made a model from a modulation circuit.

3 Implementation

To test a MOSFET transistor in modulation mode there are 3 forms of connection which is presented in the figures 3, 4 and 5.

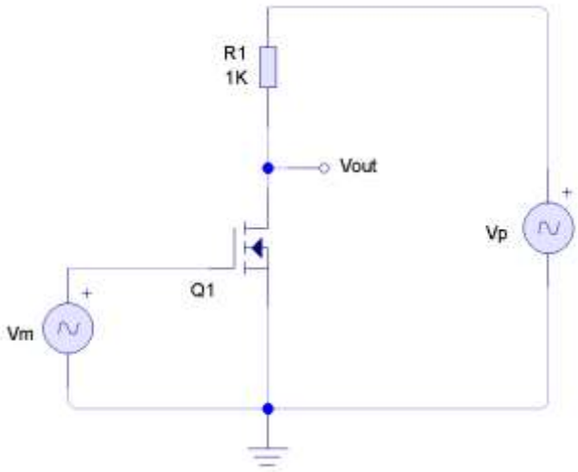

Figure 3 Connection 1, carrier signal to Drain and modulating singal to Gate
Source: PCB Wizard

In figure 3 the carrier signal is applied to the drain of the transistor, while the modulating or information signal is applied to gate, in this form take advantage of the no linear regions of the transistor. The output signal V_{out} is the carrier modulated by the signal coming from the gate.

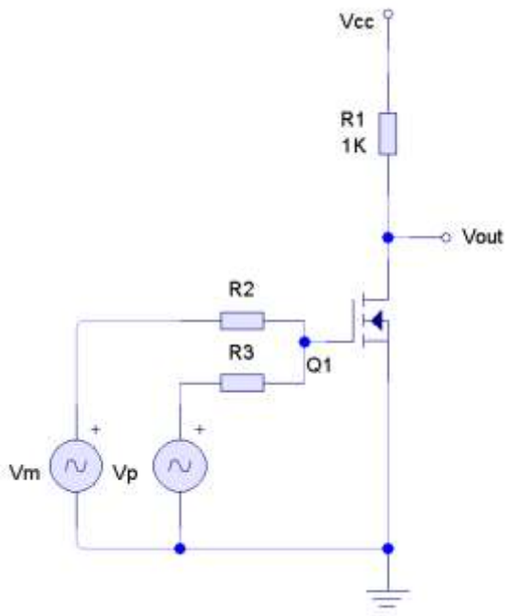

Figure 4 Connection 2, carrier and modulating signals to Gate, V_{DC} to Drain
Source: PCB Wizard.

In the figure 4 an arrangement is presented where is applied a direct voltage V_{CC} to the drain of the transistor, however in the Gate is applied the sum of the carrier signal and the modulating signal, obtaining in Vout a signal that consist the harmonics of the sum of these signals.

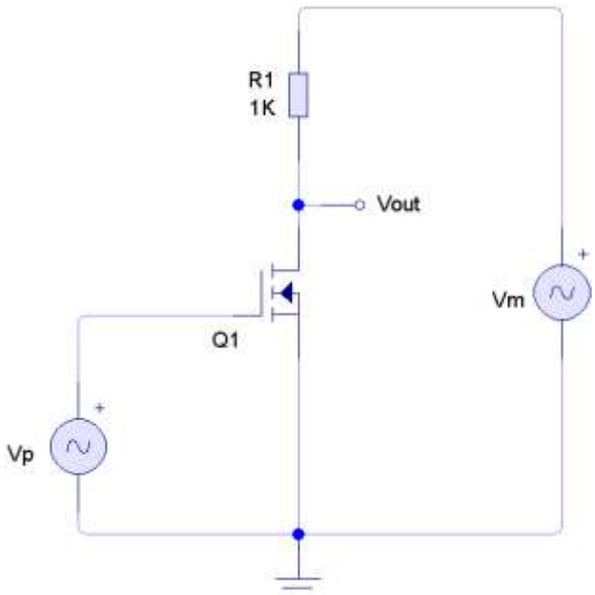

Figure 5 Connection 3, Carrier signal to Gate and modulating signal to Drain.
Source: PCB Wizard.

In the figure 5 the connections of the modulator circuit are similar to figure 3 with the difference in connection change of the signals in the transistor, for this case, the modulating signal is applied to Drain of the transistor and the carrier signal is applied to Gate.

The amplitude of the modulated signal in the circuit of figure 3 is greater than that obtained by the circuit of figure 5. In the arrangements of figures 4 and 5 the best results are obtained with the difference that in figure 4 use more elements.

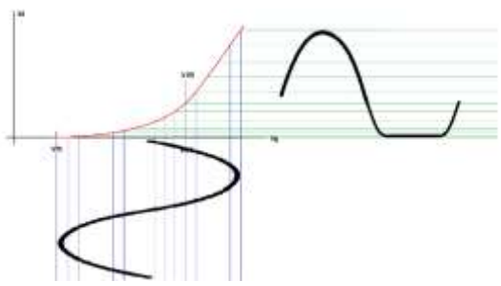

Figure 6 Drain current as a function of transistor gate voltage
Source: Own Elaboration

ISSN 2523-6776

In the figure 6 shows the ideal behavior of a MOSFET transistor, the curve that represent a quadratic expression (similar to an exponential) represents the drain current Id as a function of the gate voltage Vg.

A MOSFET transistor has 3 types of operation:

3.1 Cutting region

In this mode of operation happens when the voltage Vgs is less than Vth, this means that the enrichment channel is not formed, therefore there is no current from drain to source.

3.2 Saturation or active region

This mode of operation happens when the voltage Vgs is between Vth and VDS and this region is purely quadratic, this is due the enrichment channel is formed but not completely, that means, when Vgs increases, the channel will form according to the field electrical increase.

3.3 Lineal or ohmic region

It happens when VDS is greater than Vgs, this region is linear or ohmic because the channel is completely formed and the linear zone ascends with a positive slope. Where Kn is a parameter given by the manufacturer, which involves the dimensions of the channel as well as the electrical characteristics [6]. According to what is established in previous paragraphs, we can summarize the behavior of a MOSFET transistor as follows:

$$I_d = \begin{cases} I_{d0} e^{\frac{V_g - V_{th}}{nV_t}} & V_{th} > V_g \\ K_n\left[2(V_g - V_{th})V_{ds} - V_{ds}^2\right] & V_{th} < V_g < V_{ds} \\ K_n(V_g - V_{th})^2 & V_g > V_{ds} \end{cases} \quad (1)$$

With the help of figure 6, it is possible to have an idea of how the drain current behaves according to the connections of figures 4, 5 and 6. To use many transistors and make the tests that allows to obtain a model, was developed a fixture which is a 4x4 cm PCB designed in the programs Livewire and PCB Wizard, it is possible to polarize and add the input signal, as well as to measure the signals of interest and the substitution of the transistor for the different tests, this fixture is shown in figure 7.

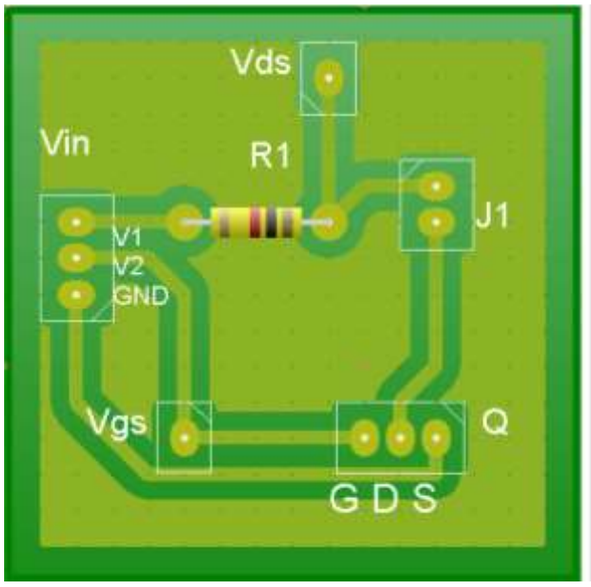

Figure 7 PCB design
Source: PCB Wizard.

The connection points Vin and Q are by means of 3-terminal headers, where Q relates to the terminals for the test transistor and Vin the bias. Vds, Vgs and J1 are male header connectors. The Vgs and Vds connectors are used to make measurements easily, while J1 is a jumper that is used to measure the current flowing through the drain of the transistor.

4. Results

Once the fixture was implemented, the circuit was polarized using the method of connecting (figure 4), with which measurements were made to the transistors described in table 1. These Measurements, previously, were made with variations in Vg from 0V to 5V with increments of 0.01V tabulating and graphing the results.

Parameters	Qgs	Ciss	Vth
RFP2N08	-	200 pF	2 a 4V
IRF9Z10	3.8 nC	270 pF	-2 a -4V
2N60B	2.2 nC	380-490 pF	2 a 4V
IRL3303	8.8 nC	870 pF	1V min*
IRF640N	11 nC	1160 pF	2 a 4V
IRF640C	13 nC	1300 pF	2 a 4V
K3878	34 nC	2200 pF	2 a 4V

Table 1 Comparative of analyzed transistors
*Source: Own acquisition. * $V_{ds} = V_{gs}$, $I_d = 250\mu A$*

As an example of the measurements carried out, the following cases are presented as representative of the work:

4.1 Measurements of parameters using K3878 TOSHIBA transistor

The experiment was made with a circuit adding the K3878 MOSFET increasing the gate-to-source voltage by 0.01V starting from 0V and ending at 5V. The circuit was polarized with Vcc = 5V in direct and values were taken in the parameters Vgs, Ids, Vds and leading to the graphical interpretations that are presented in graph 1.

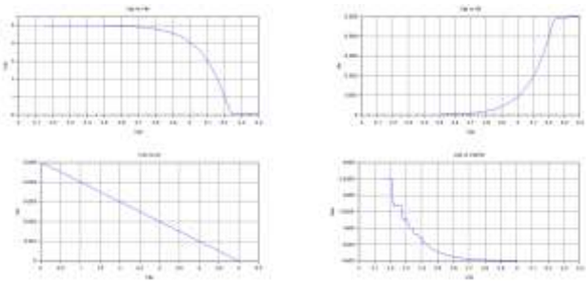

Graph 1 transistor parameters from left to right: V_{gs} vs V_{ds}, V_{gs} vs I_{ds}, V_{ds} vs I_{ds} , V_{gs} vs (V_{ds} / I_{ds})
Source: Scilab.

In the graph 1 shows the input and output characteristics of K3878 MOSFET transistor, for example transfer function of voltage (top left graph), transfer function of current (top right graph), output resistance (lower left graph) and transfer function of output resistance (lower right graph).

4.2 Measurements of parameters using IRF640N transistor

Applying the same procedure of data collection but substituting the MOSFET K3878 by IRF640N, the results is obtained that is presented in the graph 2.

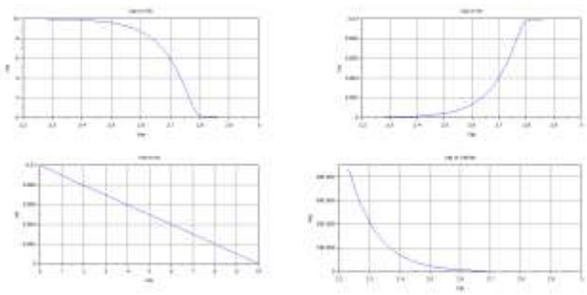

Graph 2 transistor parameters from left to right: V_{gs} vs V_{ds}, V_{gs} vs I_{ds}, V_{ds} vs I_{ds}, V_{gs} vs (V_{ds} / I_{ds})
Source: Scilab

In the graph 2 shows the input and output characteristics of IRF640N MOSFET transistor, for example transfer function of voltage (top left graph), transfer function of current (top right graph), output resistance (lower left graph) and transfer function of output resistance (lower right graph). Comparing the graphs 1 and 2 it can observe that the voltage threshold in both transistors is different, as well as is indicated in the table 1 and both transistors reach to lineal region long before of $V_{ds.}$

4.3 Comparison of measurements with theory

To make the comparison between the literature indicates with the obtained data from measurements, its necessary take as reference the measurements obtained from K3878 TOSHIBA as shown in the graph 3.

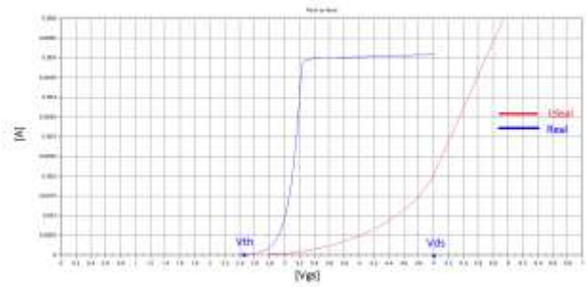

Graph 3 Comparison of transistor K3878 with an ideal behavior.
Source: Scilab

In the graph 3 the exponential line that is to the right of the graph represents the behavior of an ideal MOSFET transistor according to the literature and represented in equation (1). This behavior indicates that there is a quadratic no linear region when Vgs is between Vth and Vds. When Vgs is greater than Vds, the transistor channel is formed proportionally to Vgs, that is why the corresponding exponential growth, however, when data is captured and transferred to a graph, it is identified that the behavior of the transistor does not comply with was expressed in equation (1), giving a representation that is closer to the origin (a lower Vgs).

Observing both behaviors (transistor K378 and IRF640N) the conclusion is that a real transistor does not behave as the theory explains, also the transistor reaches the ohmic region long before Vds and the no linear behavior is not presented as a Quadratic function, for which the opportunity arises to identify the mathematical models that represent the device, for this, are used some techniques mentioned above.

ISSN 2523-6776

4.4 Polynomial equations in region of transistor K3878

Due to what was presented in the behavior of the K3878 transistor, it was proceeded to find the polynomial or exponential equations that could represent its behavior and allow a characterization of the transistor as approximately as possible to its operation, for this, it was necessary to use the trend line of Libre Office spreadsheet.

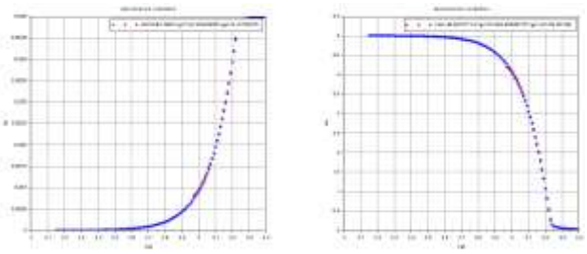

Graph 4 Quadratic approximation I_{ds} vs V_{gs} (left) y V_{ds} vs V_{gs} (right)
Source: Scilab.

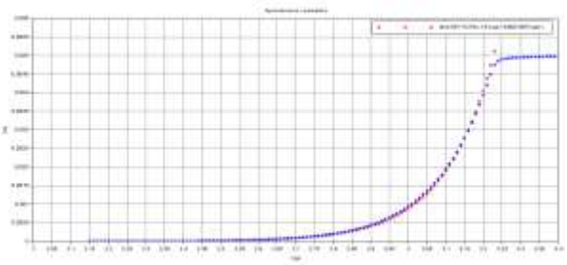

Graph 5 Exponential approximation I_{ds} vs V_{gs}
Source: Scilab

In the graph 4 it is identified that it is possible to approximate with a quadratic function a section of the behavior of the transistor, however it does not correspond to what is described in equation (1), the theory explains that the quadratic region of a MOSFET transistor is located between Vth and Vds and in graph 4 this is out the limits in theory. moreover it is possible to model the same behavior with an exponential function, covering all the no linear region, which is desirable and does not correspond to an ideal behavior.

4.5 Relation of deformation of output signal as function of frequency of the transistor

An interesting point observed in the measurements is the signal deformation of the transistor in Vds and Ids, as a function of frequency, identifying that this deformation is directly proportional to the applied frequency in Vgs,

Therefore it is necessary a investigation process of the variables involved that allow to identify the behavior.

For this experiment were used the transistors presented in table 1. These were tested using a value of

$$Vgs = 2.5sin(2\pi 200000t) + 2.5V_{dc} \quad (2)$$

with a bias V_{cc}= 5V and using the connection in the figure 4.

For this investigation the results obtained re resented as the best and worst performance, in terms of signal deformation. The best performance was presented by the RFP2N08 transistor as shown in figure 8, while the worst performance was obtained with the 2N60B transistor as shown in figure 9.

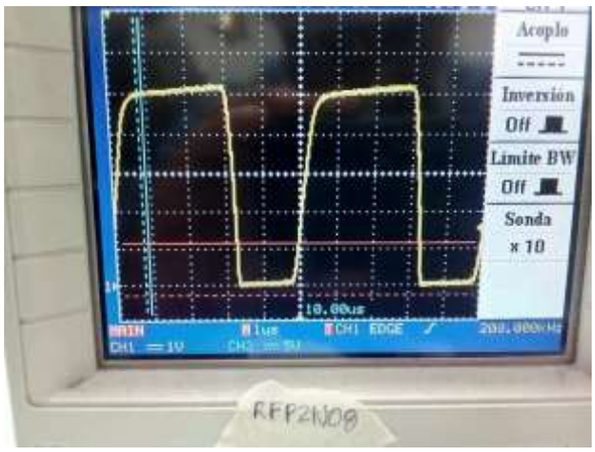

Figure 8 Deformity due to frequency of RFP2N08 transistor
Source: Own acquisition.

Figure 9 Deformity due to frequency of 2N60B transistor
Source: Own acquisition.

The performance of these transistors was compared from best to worst to find which are the variables involved in the deformation of the signal as a function of frequency. Analyzing and reading the datasheets of each of the transistors in Table 1, the variables were found that correspond to Qgs and Ciss.

According to table 1 and the previous measurements, it is concluded that the deformation as a function of the frequency of a MOSFET transistor is inversely proportional to the value of Qgs or Ciss, it means, when more small are these two values, the frequency that the transistor can handle without deforming is greater as shown in graph 6.

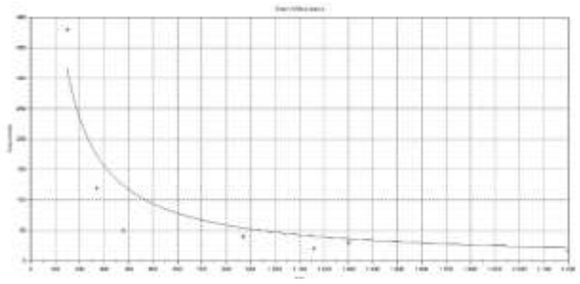

Graph 6 Relation between C_{iss} and frequency in Gate without deformation
Source: Scilab.

Graph 6 shows the relationship of a MOSFET transistor with the internal capacitance of the channel with respect to the maximum frequency that the gate can handle without deformation, preserving the characteristics of the transistor.

$$f_t = \frac{a_0}{C_{iss}} \quad (3)$$

where f_t is the frequency transistor y a_0 is the coefficient obtained by least square model.

4.6 Deformation of V_{ds} as function of the frequency

The behavior of the transistor (RFP2N08) is presented as a case study with the value of Vgs presented in expression (2), making variations in the frequency of the signal with steps of 10 KHz between each test from 25 KHz (25, 35, 45, 55, 65 KHz) highlighting the deformity of the Vds output signal.

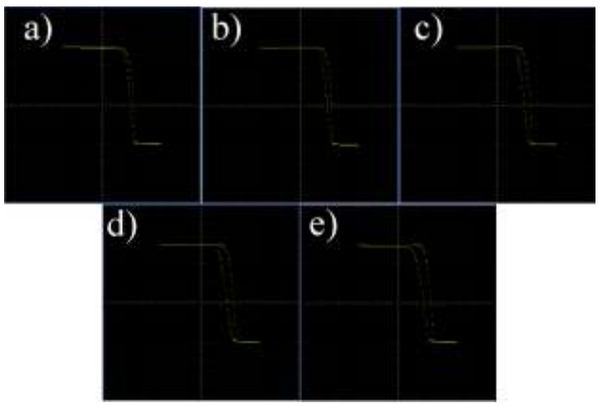

Graph 7 From left to right V_{ds} signal with 25, 35, 45, 55 y 65 KHz respectively
Source: Tektronix MDO3024

To proceed with obtaining the transistor model, the signal defined in (2) with a frequency of 45KHz for the RFP2N08 transistor, obtaining the numerical data and its graph as shown in graph 8.

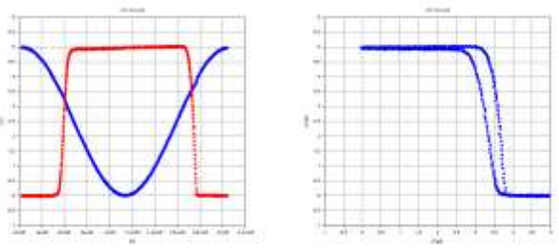

Graph 8 V_{ds} signal with 45KHz using a osciloscope as data acquisition
Source: Tektronix MDO3024.

Different linearizable numerical mathematical models were tested using the least squares method programmed in Scilab, obtaining the following model:

$$V_{ds} = \sum_{n=0}^{13} a_n \, v_{gs}{}^n \quad (4)$$

Where a_n are the coefficient obtained by the last square model which approximate the V_{ds} function.

Equation 4 represents the Vds output as the sum of powers, which is valid up to power number 13.

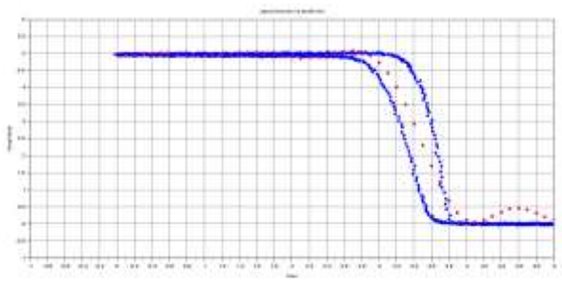

Graph 9 Comparison of the output voltage Vds (blue line) respect to the mathematical model (red dotted line)
Source: Scilab.

One of the advantages of the numerical approximation is that it considers a large part of the no linear region of the Vds signal, as well as that it is a more compact mathematical model, however it is not very exact because the model approximates to the no linear region that contains two different values, also, the model is only valid until you do not oscillate. Therefore, it was necessary to find other numerical models, being identified as pertinent by Fourier Series, which the corresponding characteristic polynomial was obtained, remaining as:

$$V_{ds} = a_0 + \sum_{n=1}^{5} a_n \cos(2\pi 45000nt) + a_{n+1}\sin(2\pi 45000nt) \quad (5)$$

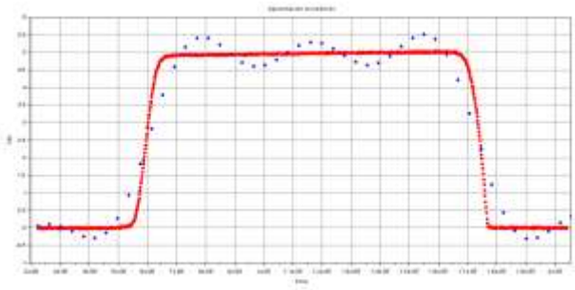

Graph 10 Comparison of the Vds output signal of the model (5) (oscillating line in blue) with the real measurement (almost continuous line in red)
Source: Scilab

4.7 Frequency domain of transistor harmonics

For the test of this model, the same procedure was followed that was obtained by least squares, with a carrier signal as the one presented in equation (2), with frequency of 45 KHz and applying the model presented in (5), as well as the analysis with FFT (fast Fourier transform) resulting in what is presented in graph 11.

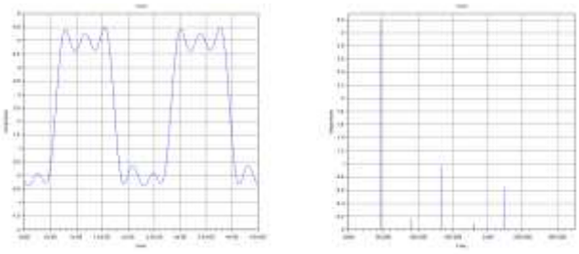

Graph 11 V_{ds} modeling and frequency spectrum
Source: Scilab.

The model (5) does not approximate the no linear region of the Vds signal that present in the temporal domain compared with the model (4). In the frequency domain due to the harmonics of model (5) it is a good candidate to be used as an AM modulator because it describes more harmonics than are necessary for modulation. The model (5) is more compact and simple but without many harmonics. Analyzing the model (4) and applying a signal like the one presented in (2) with 45 Khz and applying FFT:

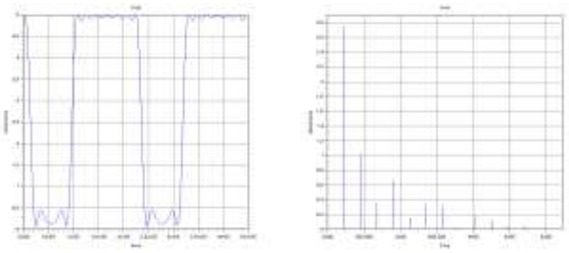

Graph 12 V_{ds} modeling and frequency spectrum
Source: Scilab.

Comparing graphs 11 and 12 the conclusion found is the model (4) is the only that is approximated to the Vds signal since it handles the sum of powers and these add more necessary harmonics. In graph 12 there are more harmonics which do not appear in graph 11.

Another numerical model was proposed for Vds as a function of Vgs, taking one of the two hysteresis lines of the transistor that is most stable in frequency changes in blue color (Graph 8), modeling only the no linear region and applying an analysis with FFT. The numerical approximation model for the no linear section of Vds as a function of Vgs is

$$V_{ds} = \sum_{n=0}^{6} a_n \, v_{gs}{}^n \quad (6)$$

ISSN 2523-6776

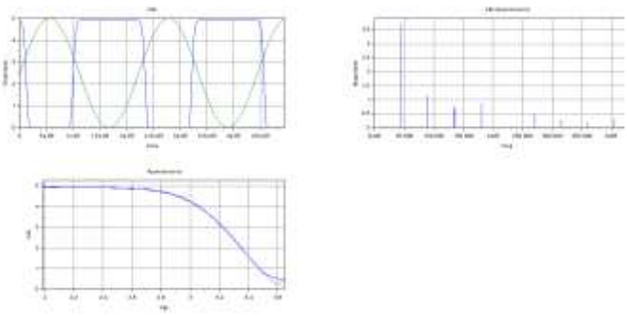

Graph 13 V_{ds} modeling and frequency spectrum using only the no linear region
Source: Scilab.

The model (6) presents a greater approximation in the temporal and frequency domain and with less processes compared to model (4) because some harmonics do not appear and they do not approximate with the results of Graph 14.

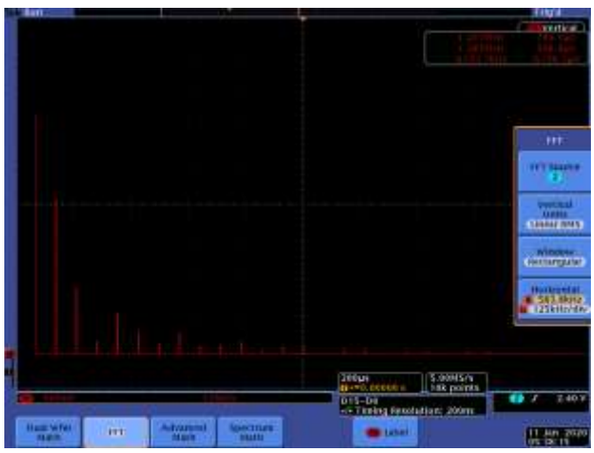

Graph 14 Measured frequency spectrum of the transistor
Source: Tektronix MDO3024

Gratitude

To the Autonomous University of Baja California and especially to the Faculty of Chemical Sciences and Engineering and to my advisor for contributing with the materials and equipment necessary to make the corresponding tests to develop this research.

Conclusions

The present work has allowed to identify that the traditional model of a MOSFET is not the only model or the most approximated to a real device, that is possible to have different approximations with a greater or lesser degree of approximation and that it is posible to make in voltage and in frequency, depending on the mathematical model as a polynomial algebraic model or a combination of transcendent functions.

Obtaining a suitable mathematical model transistor it is possible to use it for specific applications such as an AM modulator.

References

[1] Tomasi, W. (2003). Sistemas de comunicaciones electrónicas. Pearson educación.

[2] Sauer, T., & Murrieta, J. E. M. (2013). Análisis numérico . Pearson Educación.

[3] Chapra, S. C., Canale, R. P., Ruiz, R. S. G., Mercado, V. H. I., Díaz, E. M., & Benites, G. E. (2011). Métodos numéricos para ingenieros (Vol. 5). McGraw-Hill.

[4] Vidal,M.[Uniersitat Politecnica de Valncia – UPV].(2017,octubre,4)Una introducción al ajuste polinómico de datos por mínimos cuadrados, utilizando Matlab | | UPV.[Archivo de video].Recuperado de youtube.com/watch?v=d2wGLqWyoKg

[5] Bocco, M. (2010). Funciones elementales para construir modelos matemáticos.

[6] Neamen, D. A. (2007). Microelectronics: circuit analysis and design (Vol. 43). New York: McGraw-Hill.

Gerald, C. F. (1987). Análisis numérico. Representaciones y Servicios de Ingeniería.

Burden, R. L., Faires, J. D., & Iriarte Balderrama, R. (1996).Análisis numérico.

ISSN 2523-6776

Title in Times New Roman and Bold No. 14 in English and Spanish]

Surname (IN UPPERCASE), Name 1st Author†*, Surname (IN UPPERCASE), Name 1st Coauthor, Surname (IN UPPERCASE), Name 2nd Coauthor and Surname (IN UPPERCASE), Name 3rd Coauthor

Institutional Affiliation of Author including Dependency (No.10 Times New Roman and Italic)

International Identification of Science - Technology and Innovation

ID 1st Author: (ORC ID - Researcher ID Thomson, arXiv Author ID - PubMed Author ID - Open ID) and CVU 1st author: (Scholar-PNPC or SNI-CONACYT) (No.10 Times New Roman)

ID 1st Coauthor: (ORC ID - Researcher ID Thomson, arXiv Author ID - PubMed Author ID - Open ID) and CVU 1st coauthor: (Scholar or SNI) (No.10 Times New Roman)

ID 2nd Coauthor: (ORC ID - Researcher ID Thomson, arXiv Author ID - PubMed Author ID - Open ID) and CVU 2nd coauthor: (Scholar or SNI) (No.10 Times New Roman)

ID 3rd Coauthor: (ORC ID - Researcher ID Thomson, arXiv Author ID - PubMed Author ID - Open ID) and CVU 3rd coauthor: (Scholar or SNI) (No.10 Times New Roman)

(Report Submission Date: Month, Day, and Year); Accepted (Insert date of Acceptance: Use Only ECORFAN)

Abstract (In English, 150-200 words)

Objectives
Methodology
Contribution

Abstract (In Spanish, 150-200 words)

Objectives
Methodology
Contribution

Keywords (In English)

Indicate 3 keywords in Times New Roman and Bold No. 10

Keywords (In Spanish)

Indicate 3 keywords in Times New Roman and Bold No. 10

Citation: Surname (IN UPPERCASE), Name 1st Author, Surname (IN UPPERCASE), Name 1st Coauthor, Surname (IN UPPERCASE), Name 2nd Coauthor and Surname (IN UPPERCASE), Name 3rd Coauthor. Paper Title. Journal of Technological Engineering. Innovation. Year 1-1: 1-11 [Times New Roman No.10]

* Correspondence to Author (example@example.org)
† Researcher contributing as first author.

Introduction

Text in Times New Roman No.12, single space.

General explanation of the subject and explain why it is important.

What is your added value with respect to other techniques?

Clearly focus each of its features

Clearly explain the problem to be solved and the central hypothesis.

Explanation of sections Article.

Development of headings and subheadings of the article with subsequent numbers

[Title No.12 in Times New Roman, single spaced and bold]

Products in development No.12 Times New Roman, single spaced.

Including graphs, figures and tables-Editable

In the article content any graphic, table and figure should be editable formats that can change size, type and number of letter, for the purposes of edition, these must be high quality, not pixelated and should be noticeable even reducing image scale.

[Indicating the title at the bottom with No.10 and Times New Roman Bold]

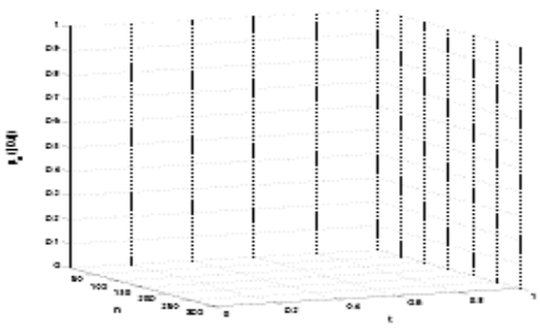

Graphic 1 Title and *Source (in italics)*

Should not be images-everything must be editable.

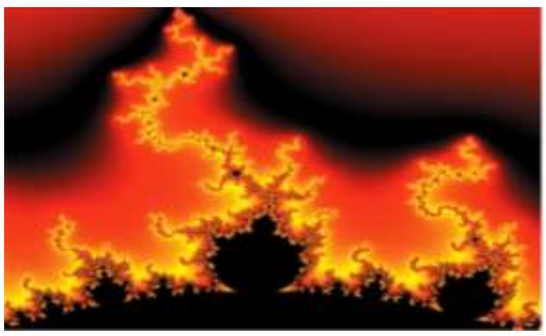

Figure 1 Title and *Source (in italics)*

Should not be images-everything must be editable.

Table 1 Title and *Source (in italics)*

Should not be images-everything must be editable.

Each article shall present separately in **3 folders**: a) Figures, b) Charts and c) Tables in .JPG format, indicating the number and sequential Bold Title.

For the use of equations, noted as follows:

$$Y_{ij} = \alpha + \sum_{h=1}^{r} \beta_h X_{hij} + u_j + e_{ij} \qquad (1)$$

Must be editable and number aligned on the right side.

Methodology

Develop give the meaning of the variables in linear writing and important is the comparison of the used criteria.

Results

The results shall be by section of the article.

Annexes

Tables and adequate sources

Thanks

Indicate if they were financed by any institution, University or company.

ISSN 2523-6776

Conclusions

Explain clearly the results and possibilities of improvement.

References

Use APA system. Should not be numbered, nor with bullets, however if necessary numbering will be because reference or mention is made somewhere in the Article.

Use Roman Alphabet, all references you have used must be in the Roman Alphabet, even if you have quoted an Article, book in any of the official languages of the United Nations (English, French, German, Chinese, Russian, Portuguese, Italian, Spanish, Arabic), you must write the reference in Roman script and not in any of the official languages.

Technical Specifications

Each article must submit your dates into a Word document (.docx):

Journal Name
Article title
Abstract
Keywords
Article sections, for example:

1. Introduction
2. Description of the method
3. Analysis from the regression demand curve
4. Results
5. Thanks
6. Conclusions
7. References

Author Name (s)
Email Correspondence to Author
References

Intellectual Property Requirements for editing:

-Authentic Signature in Color of Originality Format Author and Coauthors

-Authentic Signature in Color of the Acceptance Format of Author and Coauthors

ISSN 2523-6776

Reservation to Editorial Policy

Journal of Technological Engineering reserves the right to make editorial changes required to adapt the Articles to the Editorial Policy of the Research Journal. Once the Article is accepted in its final version, the Research Journal will send the author the proofs for review. ECORFAN® will only accept the correction of errata and errors or omissions arising from the editing process of the Research Journal, reserving in full the copyrights and content dissemination. No deletions, substitutions or additions that alter the formation of the Article will be accepted.

Code of Ethics - Good Practices and Declaration of Solution to Editorial Conflicts

Declaration of Originality and unpublished character of the Article, of Authors, on the obtaining of data and interpretation of results, Acknowledgments, Conflict of interests, Assignment of rights and Distribution

The ECORFAN-Mexico, S.C Management claims to Authors of Articles that its content must be original, unpublished and of Scientific, Technological and Innovation content to be submitted for evaluation.

The Authors signing the Article must be the same that have contributed to its conception, realization and development, as well as obtaining the data, interpreting the results, drafting and reviewing it. The Corresponding Author of the proposed Article will request the form that follows.

Article title:

– The sending of an Article to Journal of Technological Engineering emanates the commitment of the author not to submit it simultaneously to the consideration of other series publications for it must complement the Format of Originality for its Article, unless it is rejected by the Arbitration Committee, it may be withdrawn.

– None of the data presented in this article has been plagiarized or invented. The original data are clearly distinguished from those already published. And it is known of the test in PLAGSCAN if a level of plagiarism is detected Positive will not proceed to arbitrate.

– References are cited on which the information contained in the Article is based, as well as theories and data from other previously published Articles.

– The authors sign the Format of Authorization for their Article to be disseminated by means that ECORFAN-Mexico, S.C. In its Holding Taiwan considers pertinent for disclosure and diffusion of its Article its Rights of Work.

– Consent has been obtained from those who have contributed unpublished data obtained through verbal or written communication, and such communication and Authorship are adequately identified.

– The Author and Co-Authors who sign this work have participated in its planning, design and execution, as well as in the interpretation of the results. They also critically reviewed the paper, approved its final version and agreed with its publication.

– No signature responsible for the work has been omitted and the criteria of Scientific Authorization are satisfied.

– The results of this Article have been interpreted objectively. Any results contrary to the point of view of those who sign are exposed and discussed in the Article.

Copyright and Access

The publication of this Article supposes the transfer of the copyright to ECORFAN-Mexico, SC in its Holding Taiwan for its Journal of Technological Engineering, which reserves the right to distribute on the Web the published version of the Article and the making available of the Article in This format supposes for its Authors the fulfilment of what is established in the Law of Science and Technology of the United Mexican States, regarding the obligation to allow access to the results of Scientific Research.

Article Title:

Name and Surnames of the Contact Author and the Coauthors	Signature
1.	
2.	
3.	
4.	

Principles of Ethics and Declaration of Solution to Editorial Conflicts

Editor Responsibilities

The Publisher undertakes to guarantee the confidentiality of the evaluation process, it may not disclose to the Arbitrators the identity of the Authors, nor may it reveal the identity of the Arbitrators at any time.

The Editor assumes the responsibility to properly inform the Author of the stage of the editorial process in which the text is sent, as well as the resolutions of Double-Blind Review.

The Editor should evaluate manuscripts and their intellectual content without distinction of race, gender, sexual orientation, religious beliefs, ethnicity, nationality, or the political philosophy of the Authors.

The Editor and his editing team of ECORFAN® Holdings will not disclose any information about Articles submitted to anyone other than the corresponding Author.

The Editor should make fair and impartial decisions and ensure a fair Double-Blind Review.

Responsibilities of the Editorial Board

The description of the peer review processes is made known by the Editorial Board in order that the Authors know what the evaluation criteria are and will always be willing to justify any controversy in the evaluation process. In case of Plagiarism Detection to the Article the Committee notifies the Authors for Violation to the Right of Scientific, Technological and Innovation Authorization.

Responsibilities of the Arbitration Committee

The Arbitrators undertake to notify about any unethical conduct by the Authors and to indicate all the information that may be reason to reject the publication of the Articles. In addition, they must undertake to keep confidential information related to the Articles they evaluate.

Any manuscript received for your arbitration must be treated as confidential, should not be displayed or discussed with other experts, except with the permission of the Editor.

The Arbitrators must be conducted objectively, any personal criticism of the Author is inappropriate.

The Arbitrators must express their points of view with clarity and with valid arguments that contribute to the Scientific, Technological and Innovation of the Author.

The Arbitrators should not evaluate manuscripts in which they have conflicts of interest and have been notified to the Editor before submitting the Article for Double-Blind Review.

Responsibilities of the Authors

Authors must guarantee that their articles are the product of their original work and that the data has been obtained ethically.

Authors must ensure that they have not been previously published or that they are not considered in another serial publication.

Authors must strictly follow the rules for the publication of Defined Articles by the Editorial Board.

The authors have requested that the text in all its forms be an unethical editorial behavior and is unacceptable, consequently, any manuscript that incurs in plagiarism is eliminated and not considered for publication.

Authors should cite publications that have been influential in the nature of the Article submitted to arbitration.

Information services

Indexation - Bases and Repositories

RESEARCH GATE (Germany)
GOOGLE SCHOLAR (Citation indices-Google)
MENDELEY (Bibliographic References Manager)
REDIB (Ibero-American Network of Innovation and Scientific Knowledge- CSIC)
HISPANA (Information and Bibliographic Orientation-Spain)

Publishing Services

Citation and Index Identification H
Management of Originality Format and Authorization
Testing Article with PLAGSCAN
Article Evaluation
Certificate of Double-Blind Review
Article Edition
Web layout
Indexing and Repository
ArticleTranslation
Article Publication
Certificate of Article
Service Billing

Editorial Policy and Management

69 Street. YongHe district, ZhongXin. Taipei-Taiwan. Phones: +52 1 55 6159 2296, +52 1 55 1260 0355, +52 1 55 6034 9181; Email: contact@ecorfan.org www.ecorfan.org

Journal of Technological Engineering

2523 6776
ISSN 2523 - 6776

www.ecorfan.org